The concept that a nonfibrillar precursor of amyloid can exert toxic effects can be extended to other pathologic conditions where amyloid is considered pathogenetically important, including Alzheimer disease.[42-45] In our study, amyloid was not deposited in late-onset cases until patients had become elderly, considering that amyloid deposition was scarce or absent in sural nerve biopsy specimens. Accumulation of amyloid may progress rapidly once initiated. Abundant nerve fiber regeneration despite scarce amyloid deposition was observed in most sural nerve biopsy specimens from our late-onset cases, indicating that axons had been degenerating long before amyloid deposition occurred in these cases. At autopsy, less amyloid deposition but severe myelinated fiber loss in nerve trunks from a late-onset case in comparison with early-onset cases support this view. Furthermore, amorphous material staining with anti-transthyretin antibody but not with Congo red, indicating presence of the nonfibrillar amyloid precursor, was more abundant in the late-onset case. Taken together, these observations support cytotoxicity from nonfibrillar transthyretin affecting all sizes of axons and neurons prior to deposition of congophilic amyloid in late-onset cases. In early-onset cases, amyloid deposition was likely to have been severe even in early stages, judging from amounts of amyloid observed. Nerve fiber compression by amyloid deposits could cause predominantly small-fiber loss, as previously suggested.[26] Differential duration of exposure to a toxic amyloid precursor may result in pathologically different modes of axonal and neuronal cell loss.

## References


1. Andrade C. A peculiar form of peripheral neuropathy. Familial atypical generalized amyloidosis with special involvement of the peripheral nerves. Brain 1952;75:408–427.
2. Benson MD, Cohen AS. Generalized amyloid in a family of Swedish origin. A study of 426 family members in seven generations of a new kinship with neuropathy, nephropathy, and central nervous system involvement. Ann Intern Med 1977;86:419–424.
3. Ikeda S, Hanyu N, Hongo M, et al. Hereditary generalized amyloidosis with polyneuropathy: clinicopathological study of 65 Japanese patients. Brain 1987;110:315–337.
4. Nakazato M, Shiomi K, Miyazato M, Matsukura S. Type 1 familial amyloidotic polyneuropathy in Japan. Intern Med 1992;31:1335–1338.
5. Sousa A, Coelho T, Barros J, Sequeiros J. Genetic epidemiology of familial amyloidotic polyneuropathy (FAP)-type I in Povoa do Varzim and Vila do Conde (north of Portugal). Am J Med Genet 1995;60:515–521.
6. Reilly MM, Adams D, Booth DR, et al. Transthyretin gene analysis in European patients with suspected familial amyloid polyneuropathy. Brain 1995;118:849–856.
7. Ando Y, Araki S, Shimoda O, Kano T. Role of autonomic nerve functions in patients with familial amyloidotic polyneuropathy as analyzed by laser Doppler flowmetry, capsule hydrograph, and cardiographic R-R interval. Muscle Nerve 1992;15:507–512.
8. Ando Y, Suhr OB. Autonomic dysfunction in familial amyloid polyneuropathy (FAP). Amyloid Int J Exp Clin Invest 1998;5:288–300.
9. Misu K, Hattori N, Nagamatsu M, et al. Late-onset familial amyloid polyneuropathy type I (transthyretin Met 30-associated familial amyloid polyneuropathy) unrelated to endemic focus in Japan; clinicopathological and genetic features. Brain 1999;122:1951–1962.
10. Misu K, Hattori N, Ando Y, Ikeda S, Sobue G. Anticipation in early- but not late-onset familial amyloid polyneuropathy (TTR met 30) in Japan. Neurology 2000;55:451–452.
11. Koike H, Misu K, Ikeda S, et al. Type I (transthyretin Met30) familial amyloid polyneuropathy in Japan: early- versus late-onset form. Arch Neurol 2002;59:1771–1776.
12. Sobue G, Koike H, Misu K, et al. Clinicopathologic features of early- and late-onset FAP type I (FAP ATTR Val30Met) in Japan. Amyloid J Protein Folding Disord 2003;1(suppl):32–38.
13. Coelho T, Sousa A, Lourenco E, Ramalheira J. A study of 159 Portuguese patients with familial amyloidotic polyneuropathy (FAP) whose parents were both unaffected. J Med Genet 1994;31:293–299.
14. Saravia MJ, Costa PP, Goodman DS. Genetic expression of a transthyretin mutation in typical and late-onset Portuguese families with familial amyloidotic polyneuropathy. Neurology 1986;36:1413–1417.
15. Sasaki Y, Yoshioka K, Tanahashi H, Furuya H, Sasaki H. Human transthyretin (prealbumin) gene and molecular genetics of familial amyloidotic polyneuropathy. Mol Biol Med 1989;6:161–168.
16. Sobue G, Yasuda T, Mitsuma T, Loss AH, Pleasure D. Expression of nerve growth factor receptor in human peripheral neuropathies. Ann Neurol 1988;24:64–72.
17. Sobue G, Hashizume Y, Mukai E, et al. X-linked recessive bulbospinal neuronopathy, a clinicopathological study. Brain 1989;112:209–232.
18. Sobue G, Nakao N, Murakami K, et al. Type I familial amyloid polyneuropathy. A pathological study of the peripheral nervous system. Brain 1990;113:903–919.
19. Hattori N, Ichimura M, Nagamatsu M, et al. Clinicopathological features of Churg–Strauss syndrome-associated neuropathy. Brain 1999; 122:427–439.
20. Koike H, Mori K, Misu K, et al. Painful alcoholic polyneuropathy with predominant small-fiber loss and normal thiamine status. Neurology 2001;56:1727–1732.
21. Koike H, Iijima M, Sugiura M, et al. Alcoholic neuropathy is clinicopathologically distinct from thiamine-deficiency neuropathy. Ann Neurol 2003;54:19–29.
22. Hattori N, Yamamoto M, Yoshihara T, et al. Demyelinating and axonal features of Charcot–Marie–Tooth disease with mutations of myelin-related proteins (PMP22, MPZ and Cx32): a clinicopathological study of 205 Japanese patients. Brain 2003;126:134–151.
23. Dyck PJ, Giannini C, Lais A. Pathologic alterations of nerves. In: Dyck PJ, Thomas PK, Griffin JW, Low PA, Poduslo JF, eds. Peripheral neuropathy. 3rd ed. Philadelphia: Saunders, 1993:514–595.
24. Nagamatsu M, Terao S, Misu K, et al. Axonal and perikaryal involvement in chronic inflammatory demyelinating polyneuropathy. J Neurol Neurosurg Psychiatry 1999;66:727–733.
25. Takahashi K, Sakashita N, Ando Y, Suga M, Ando M. Late onset type I familial amyloidotic polyneuropathy: presentation of three autopsy cases in comparison with 19 autopsy cases of the ordinary type. Pathol Int 1997;47:353–359.
26. Said G, Ropert A, Faux N. Length-dependent degeneration of fibers in Portuguese amyloid polyneuropathy: a clinicopathologic study. Neurology 1984;34:1025–1032.
27. Takahashi K, Yi S, Kimura Y, Araki S. Familial amyloidotic polyneuropathy type 1 in Kumamoto, Japan: a clinicopathologic, histochemical, immunohistochemical, and ultrastructural study. Hum Pathol 1991;22: 519–527.
28. Olson LJ, Gertz MA, Edwards WD, et al. Senile cardiac amyloidosis with myocardial dysfunction. Diagnosis by endomyocardial biopsy and immunohistochemistry. N Engl J Med 1987;317:738–742.
29. Tashima T, Kitamoto T, Tateishi J, Ogomori K, Nakagaki H. Incidence and characterization of age related amyloid deposits in the human anterior pituitary gland. Virchows Arch A Pathol Anat Histopathol 1988;412:323–327.
30. Röcken C, Eick B, Saeger W. Senile amyloidosis of the pituitary and adrenal glands. morphological and statistical investigations. Virchows Arch 1996;429:293–299.
31. Westermark P, Eriksson L, Engstrom U, Enestrom S, Sletten K. Prolactin-derived amyloid in the aging pituitary gland. Am J Pathol 1997;150:67–73.
32. Magnus JH, Stenstad T. Proteoglycans and the extracellular matrix in amyloidosis. Amyloid J Exp Clin Invest 1997;4:121–134.
33. Nakayama Y, Narita T, Mori A, Uesaka S, Miyazaki K, Ito H. The effects of age and sex on chondroitin sulfates in normal synovial fluid. Arthritis Rheum 2002;46:2105–2108.
34. Carrino DA, Onnerfjord P, Sandy JD, et al. Age-related changes in the proteoglycans of human skin. Specific cleavage of decorin to yield a major catabolic fragment in adult skin. J Biol Chem 2003;278:17566–17572.
35. Hanyu N, Ikeda S, Nakadai A, Yanagisawa N, Powell HC. Peripheral nerve pathological findings in familial amyloid polyneuropathy: a correlative study of proximal sciatic nerve and sural nerve lesions. Ann Neurol 1989;25:340–350.
36. Berghoff M, Kathpal M, Khan F, Skinner M, Falk R, Freeman R. Endothelial dysfunction precedes C-fiber abnormalities in primary (AL) amyloidosis. Ann Neurol 2003;53:725–730.
37. Dyck PJ, Lambert EH. Dissociated sensation in amyloidosis. Compound action potential, quantitative histologic and teased-fiber, and electron microscopic studies of sural nerve biopsies. Arch Neurol 1969;20:490–507.
38. Sousa MM, Cardoso I, Fernandes R, Guimaraes A, Saraiva MJ. Deposition of transthyretin in early stages of familial amyloidotic polyneuropathy: evidence for toxicity of nonfibrillar aggregates. Am J Pathol 2001; 159:1993–2000.
39. Andersson K, Olofsson A, Nielsen EH, Svehag SE, Lundgren E. Only amyloidogenic intermediates of transthyretin induce apoptosis. Biochem Biophys Res Commun 2002;294:309–314.

40. Fiszman ML, Di Egidio M, Ricart KC, et al. Evidence of oxidative stress in familial amyloidotic polyneuropathy type 1. Arch Neurol 2003;60: 593–597.
41. Sousa MM, Fernandes R, Palha JA, Taboada A, Vieira P, Saraiva MJ. Evidence for cytotoxic aggregates in transgenic mice for human transthyretin Leu55Pro. Am J Pathol 2002;161:1935–1948.
42. LaFerla FM, Tinkle BT, Bieberich CJ, Haudenschild CC, Jay G. The Alzheimer's Abeta peptide induces neurodegeneration and apoptotic cell death in transgenic mice. Nat Genet 1995;9:21–30.
43. Hartley DM, Walsh DM, Ye CP, et al. Protofibrillar intermediates of amyloid beta-protein induce acute electrophysiological changes and progressive neurotoxicity in cortical neurons. J Neurosci 1999;19:8876–8884.
44. McLean CA, Cherny RA, Fraser FW, et al. Soluble pool of Abeta amyloid as a determinant of severity of neurodegeneration in Alzheimer's disease. Ann Neurol 1999;46:860–866.
45. Kayed R, Head E, Thompson JL, et al. Common structure of soluble amyloid oligomers implies common mechanism of pathogenesis. Science 2003;300:486–489.

THE JOURNAL OF BIOLOGICAL CHEMISTRY
Vol. 279, No. 49, Issue of December 3, pp. 51376–51385, 2004
Printed in U.S.A.


# Physical and Functional Interaction between Dorfin and Valosin-containing Protein That Are Colocalized in Ubiquitylated Inclusions in Neurodegenerative Disorders*

Received for publication, June 15, 2004, and in revised form, August 31, 2004
Published, JBC Papers in Press, September 29, 2004, DOI 10.1074/jbc.M406683200

**Shinsuke Ishigaki‡§¶, Nozomi Hishikawa‡, Jun-ichi Niwa‡, Shun-ichiro Iemura‖, Tohru Natsume‖, Seiji Hori**, Akira Kakizuka**‡‡, Keiji Tanaka§, and Gen Sobue‡§§**

*From the ‡Department of Neurology, Nagoya University Graduate School of Medicine, Nagoya 466-8500, Japan, the §Department of Molecular Oncology, Tokyo Metropolitan Institute of Medical Science, Tokyo 113-8613, Japan, the ‖National Institute of Advanced Science and Technology, Biological Information Research Center, Tokyo 135-0064, Japan, the **Laboratory of Functional Biology, Kyoto University Graduate School of Biostudies, Kyoto 606-8502, Japan, and ‡‡CREST, Japan Science and Technology Agency, Kawaguchi 332-0012, Japan*

**Dorfin, a RING-IBR type ubiquitin ligase (E3), can ubiquitylate mutant superoxide dismutase 1, the causative gene of familial amyotrophic lateral sclerosis (ALS). Dorfin is located in ubiquitylated inclusions (UBIs) in various neurodegenerative disorders, such as ALS and Parkinson's disease (PD). Here we report that Valosin-containing protein (VCP) directly binds to Dorfin and that VCP ATPase activity profoundly contributes to the E3 activity of Dorfin. High through-put analysis using mass spectrometry identified VCP as a candidate of Dorfin-associated protein. Glycerol gradient centrifugation analysis showed that endogenous Dorfin consisted of a 400–600-kDa complex and was co-immunoprecipitated with endogenous VCP. *In vitro* experiments showed that Dorfin interacted directly with VCP through its C-terminal region. These two proteins were colocalized in aggresomes in HEK293 cells and UBIs in the affected neurons of ALS and PD. $VCP^{K524A}$, a dominant negative form of VCP, reduced the E3 activity of Dorfin against mutant superoxide dismutase 1, whereas it had no effect on the autoubiquitylation of Parkin. Our results indicate that VCPs functionally regulate Dorfin through direct interaction and that their functional interplay may be related to the process of UBI formation in neurodegenerative disorders, such as ALS or PD.**

Amyotrophic lateral sclerosis (ALS)[1] is one of the most common neurodegenerative disorders, characterized by selective motor neuron degeneration in the spinal cord, brain stem, and cortex. Two genes, CuZn-superoxide dismutase (SOD1) and amyotrophic lateral sclerosis 2 have been identified as responsible genes for familial forms of ALS. Using mutant SOD1 transgenic mice, the pathogenesis of ALS has been partially uncovered. The proposed mechanisms of the motor neuron degeneration in ALS include oxidative toxicity, glutamate receptor abnormality, ubiquitin proteasome dysfunction, inflammatory and cytokine activation, dysfunction of neurotrophic factors, damage to mitochondria, cytoskeletal abnormalities, and activation of the apoptosis pathway (1, 2).

In a previous study (3), we identified several ALS-associated genes using molecular indexing. Dorfin was identified as one of the up-regulated genes in ALS, which contains a RING-IBR (in between ring finger) domain at its N terminus and mediated ubiquitin ligase (E3) activity (3, 4). Dorfin colocalized with Vimentin at the centrosome after treatment with a proteasome inhibitor in cultured cells (4). Dorfin physically bound and ubiquitylated various SOD1 mutants derived from familial ALS patients and enhanced their degradation, but it had no effect on the stability of wild-type SOD1 (5). Overexpression of Dorfin protected neural cells against the toxic effects of mutant SOD1 and reduced SOD1 inclusions (5).

Recent findings indicate that the ubiquitin-proteasome system is widely involved in the pathogenesis of Parkinson's disease (PD), Alzheimer's disease, polyglutamine disease, and Prion diseases as well as ALS (6). From this point of view, we previously analyzed the pathological features of Dorfin in various neurodegenerative diseases and found that Dorfin was predominantly localized not only in Lewy body (LB)-like inclusions in ALS but also in LBs in PD, dementia with Lewy bodies, and glial cell inclusions in multiple system atrophy (7). These characteristic intracellular inclusions composed of aggregated, ubiquitylated proteins surrounded by disorganized filaments are the histopathological hallmark of aging-related neurodegenerative diseases (8).

A structure called aggresome by Johnston *et al.* (9) is formed when the cell capacity to degrade misfolded proteins is exceeded. The aggresome has been defined as a pericentriolar, membrane-free, cytoplasmic inclusion containing misfolded ubiquitylated protein ensheathed in a cage of intermediate filaments, such as Vimentin (9). The formation of the aggresome mimics that of ubiquitylated inclusions (UBIs) in the affected neurons of various neurodegenerative diseases (10). Combined with the fact that Dorfin was localized in aggresomes in cultured cells and UBIs in ALS and other neurode-

* This work was supported by a grant for a Center of Excellence from the Ministry of Education, Culture, Sports, Science, and Technology of Japan. The costs of publication of this article were defrayed in part by the payment of page charges. This article must therefore be hereby marked "*advertisement*" in accordance with 18 U.S.C. Section 1734 solely to indicate this fact.

¶ Research resident of the Japan Foundation for Aging and Health, Psychiatric and Neurological Diseases, and Mental Health.

§§ To whom correspondence should be addressed: Dept. of Neurology, Nagoya University Graduate School of Medicine, Nagoya 466-8500, Japan. Tel.: 81-52-744-2385; Fax: 81-52-744-2384; E-mail: sobueg@med.nagoya-u.ac.jp.

[1] The abbreviations used are: ALS, amyotrophic lateral sclerosis; E3, ubiquitin ligase; ERAD, endoplasmic reticulum-associated degradation; LB, Lewy body; MS, mass spectrometry; LC-MS/MS, liquid chromatography coupled to electrospray tandem mass spectrometry; PD, Parkinson's disease; SOD1, CuZn-superoxide dismutase; UBI, ubiquitylated inclusions; VCP, valosin-containing protein; FLAG-Parkin, pcDNA3.1/FLAG-Parkin; Ub, ubiquitin; MBP, maltose-binding protein; GST, glutathione *S*-transferase; PBS, phosphate-buffered saline; HA, hemagglutinin; WT, wild type.

generative diseases, these observations suggest that Dorfin may have a significant role in the quality control system in the cell. The present study was designed to obtain further clues for the pathophysiological roles of Dorfin. For this purpose, we screened Dorfin-associated proteins using high performance liquid chromatography coupled to electrospray tandem mass spectrometry (LC-MS/MS). The results showed that Valosin-containing protein (VCP), also called p97 or Cdc48 homologue, obtained from the screening, physically and functionally interacted with Dorfin. Furthermore, both Dorfin and VCP proteins colocalized in aggresomes of the cultured cells and in UBIs in various neurodegenerative diseases.

## MATERIALS AND METHODS

*Plasmids and Antibodies*—pCMV2/FLAG-Dorfin vector (FLAG-Dorfin$^{WT}$) was prepared by PCR using the appropriate design of PCR primers with restriction sites (ClaI and KpnI). The PCR product was digested and inserted into the ClaI-KpnI site in pCMV2 vector (Sigma). pEGFP-Dorfin (GFP-Dorfin), pCMX-VCP$^{Wt}$ (VCP$^{Wt}$), and pCMX-VCP$^{K524A}$ (VCP$^{K524A}$) vectors were described previously (5, 11). pcDNA/HA-VCP$^{Wt}$ (HA-VCP$^{Wt}$) and pcDNA/HA-VCP$^{K524A}$ (HA-VCP$^{K524A}$) were subcloned from pCMX-VCP$^{Wt}$ and pCMX-VCP$^{K524A}$, respectively, into pcDNA3.1 vectors (Invitrogen). The HA tag was introduced at the N terminus of VCP. pcDNA3.1/FLAG-Parkin (FLAG-Parkin) was generated by PCR using the appropriate design of PCR primers with restriction sites (EcoRI and NotI) from pcDNA3.1/Myc-Parkin (12). The FLAG tag was introduced at the N terminus of Parkin. To establish the RING mutant plasmid of Dorfin (FLAG-Dorfin$^{C132S/C135S}$), point mutations for Cys at positions 132 and 135 to Ser were generated by PCR-based site-directed mutagenesis using a QuikChange™ site-directed mutagenesis kit (Stratagene, La Jolla, CA). pcDNA3.1/HA-Ub (HA-Ub), pcDNA3.1/Myc-SOD1$^{WT}$ (SOD1$^{WT}$-Myc), pcDNA3.1/Myc-SOD1$^{G93A}$ (SOD1$^{G93A}$-Myc), and pcDNA3.1/Myc-SOD1$^{G85R}$ (SOD1$^{G85R}$-Myc) were described previously (13, 14). Polyclonal anti-Dorfin (Dorfin-30 and Dorfin-41) and monoclonal anti-VCP antibodies were used as in previous reports (5, 15). The following antibodies were used in this study: monoclonal anti-FLAG antibody (M2; Sigma), monoclonal anti-Myc antibody (9E10; Santa Cruz Biotechnology, Santa Cruz, CA), monoclonal anti-HA antibody (12CA5; Roche Applied Science), polyclonal anti-maltose-binding protein (MBP) antibody (New England BioLabs, Beverly, MA), polyclonal anti-Parkin (Cell Signaling, Beverly, MA), and polyclonal anti-SOD1 (SOD-100; Stressgen, San Diego, CA).

*Cell Culture and Transfection*—All media and reagents for cell culture were purchased from Invitrogen. HEK293 cells were grown in Dulbecco's modified Eagle's medium containing 10% fetal calf serum, 5 units/ml penicillin, and 50 μg/ml streptomycin. HEK293 cells at subconfluence were transfected with the indicated plasmids using FuGENE6 reagent (Roche Applied Science). To inhibit cellular proteasome activity, cells were treated with 1 μM MG132 (benzyloxycarbonyl-Leu-Leu-Leu-al; Sigma) for 16 h after overnight post-transfection. Cells were analyzed at 24–48 h after transfection.

*Protein Identification by LC-MS/MS Analysis*—FLAG-Dorfin$^{WT}$ was expressed in HEK293 cells (semiconfluent in a 10-cm dish) and then immunoprecipitated by anti-FLAG antibody. The immunoprecipitates were eluted with a FLAG peptide and then digested with Lys-C endopeptidase (*Achromobacter* protease I). The resulting peptides were analyzed using a nanoscale LC-MS/MS system as described previously (16). The peptide mixture was applied to a Mightysil-PR-18 (1-μm particle, Kanto Chemical Corp., Tokyo) column (45 × 0.150 mm ID) and separated using a 0–40% gradient of acetonitrile containing 0.1% formic acid over 30 min at a flow rate of 50 nl/min. Eluted peptides were sprayed directly into a quadrupole time-of-flight hybrid mass spectrometer (Q-Tof *Ultima*; Micromass, Manchester, UK). MS and MS/MS spectra were obtained in data-dependent mode. Up to four precursor ions above an intensity threshold of 10 cps were selected for MS/MS analysis from each survey scan. All MS/MS spectra were searched against protein sequences of Swiss Prot and RefSeq (NCBI) using batch processes of the Mascot software package (Matrix Science, London, UK). The criteria for match acceptance were the following: 1) when the match score was 10 over each threshold, identification was accepted without further consideration; 2) when the difference of score and threshold was lower than 10 or when proteins were identified based on a single matched MS/MS spectrum, we manually confirmed the raw data prior to acceptance; 3) peptides assigned by less than three y series ions and peptides with +4 charge state were all eliminated regardless of their scores.

*Recombinant Proteins and Pull-down Assay*—We used pMALp2 (New England BioLabs) and pMALp2T (Factor Xa cleavage site of pMALp2 was replaced with a thrombin recognition site) to express fusion proteins with MBP. To produce the full-length (residues 1–838) Dorfin (MBP-Dorfin$^{full}$), N-terminal (residues 1–367) Dorfin (MBP-Dorfin$^{N}$), and C-terminal (residues 368–838) Dorfin (MBP-Dorfin$^{C}$), the PCR fragments were amplified from pcDNA4/HisMax-Dorfin (4) by using the appropriate PCR primers with restriction sites (FbaI and HindIII) and then ligated into pMAL-p2 vectors. To produce the MBP-Parkin protein, full-length *PARKIN* cDNA was inserted into the EcoRI-NotI sites of pMALp2T. All of the MBP-tagged recombinant proteins were purified from *Escherichia coli* BL21-codon-plus. The detail of the purification method of MBP-tagged proteins was described previously (17). Recombinant GST fusion VCP$^{WT}$ and VCP$^{K524A}$ proteins were also generated from *E. coli* lysate and purified with glutathione-Sepharose. Recombinant His-VCP$^{WT}$ and His-VCP$^{K524A}$ proteins were purified from insect cells using baculovirus. The detail of purification of these recombinant VCP proteins was described previously (15). Binding experiments were performed with proteins carrying different tags. His- or GST-VCP were mixed with MBP fusion proteins: MBP-Dorfin$^{full}$, -Dorfin$^{N}$, -Dorfin$^{C}$, -Parkin, and -mock. His-VCP and GST-VCP proteins were precipitated by $Ni^{2+}$-nitrilotriacetic acid-agarose (Qiagen, Valencia, CA), and glutathione-Sepharose (Amersham Biosciences), respectively. Binding was performed with 1–3 μg of each protein in 300 μl of binding buffer (50 mM Tris-HCl, pH 7.5, 100 mM NaCl, 5 mM $MgCl_2$, 10% glycerol, 0.5 mg/ml bovine serum albumin, 1 mM dithiothreitol) for 1 h at 4 °C. Then 15 μl of beads were added and incubated for 30 min. The beads were washed by binding buffer three times and eluted with sample buffer and analyzed by SDS-PAGE followed by Western blotting using specific antibodies.

*Glycerol Gradient Centrifugation*—Cultured cells or mouse tissues were homogenized in 1 ml of PBS with protease inhibitor (Complete Mini; Roche Applied Science). Supernatants (1 mg of protein for cultured cells, 5 mg of protein for mouse tissues, and 0.1 mg of recombinant His-VCP protein) were used as the samples after 10,000 × *g* centrifugation for 20 min. The samples (1.0 ml) were loaded on top of a 34-ml linear gradient of glycerol (10–40%) prepared in 25 mM Tris-HCl buffer, pH 7.5, containing 1 mM dithiothreitol in 40 PA centrifuge tubes (Hitachi, Tokyo), and centrifuged at 4 °C and 80,000 × *g* for 22 h using a Himac CP100α centrifuge system (Hitachi). Thirty fractions were collected from the top of the tubes. Two hundred μl of each fraction was precipitated with acetone, and the remaining pellet was lysed with 50 μl of sample buffer and then used for SDS-PAGE followed by Western blotting.

*Immunological Analysis*—Cells (4 × $10^5$ in a 6-cm dish) were lysed with 500 μl of lysis buffer (50 mM Tris-HCl, 150 mM NaCl, 1% Nonidet P-40, and 1 mM EDTA) with protease inhibitor mixture (Complete Mini) 24–48 h after transfection. The lysate was then centrifuged at 10,000 × *g* for 10 min at 4 °C to remove debris. A 10% volume of the supernatants was used as the "lysate" for SDS-PAGE. When immunoprecipitated, the supernatants were precleared with protein A-Sepharose (Amersham Biosciences), and specific antibodies, anti-FLAG (M2), anti-Myc (9E10), or anti-Dorfin (Dorfin-30) were then added and then incubated at 4 °C with rotation. Immune complexes were then incubated with protein A-Sepharose for 3 h, collected by centrifugation, and washed four times with the lysis buffer. For protein analysis, immune complexes were dissociated by heating in SDS-PAGE sample buffer and loaded onto SDS-PAGE. The samples were separated by SDS-PAGE (12% gel or 4–12% gradient gel) and transferred onto a polyvinylidene difluoride membrane. Finally, Western blotting was performed with specific antibodies.

*Immunohistochemistry*—HEK293 cells grown on glass coverslips were fixed in 4% paraformaldehyde in PBS for 15 min. Then the cells were blocked for 30 min with 5% (v/v) normal goat serum in PBS, incubated for 1 h at 37 °C with anti-HA antibody (12CA5), washed with PBS, and incubated for 30 min with Alexa 496-nm anti-mouse antibodies (Molecular Probes, Inc., Eugene, OR). The coverslips were washed and mounted on slides. Fluorescence images were obtained using a fluorescence microscope (DMIRE2; Leica, Bannockburn, IL) equipped with a cooled charge-coupled device camera (CTR MIC; Leica). Pictures were taken using Leica Qfluoro software.

*Pathological Studies*—Pathological studies were carried out on 10% formalin-fixed, paraffin-embedded spinal cords and brain stems filed in the Department of Neurology, Nagoya University Graduate School of Medicine. The specimens were obtained at autopsy from three sporadic cases of ALS and four sporadic PD patients. The spinal cord and brain stem specimens of these ALS and PD cases were immunohistochemically stained with antibodies against Dorfin (Dorfin-41) and VCP. Dou-

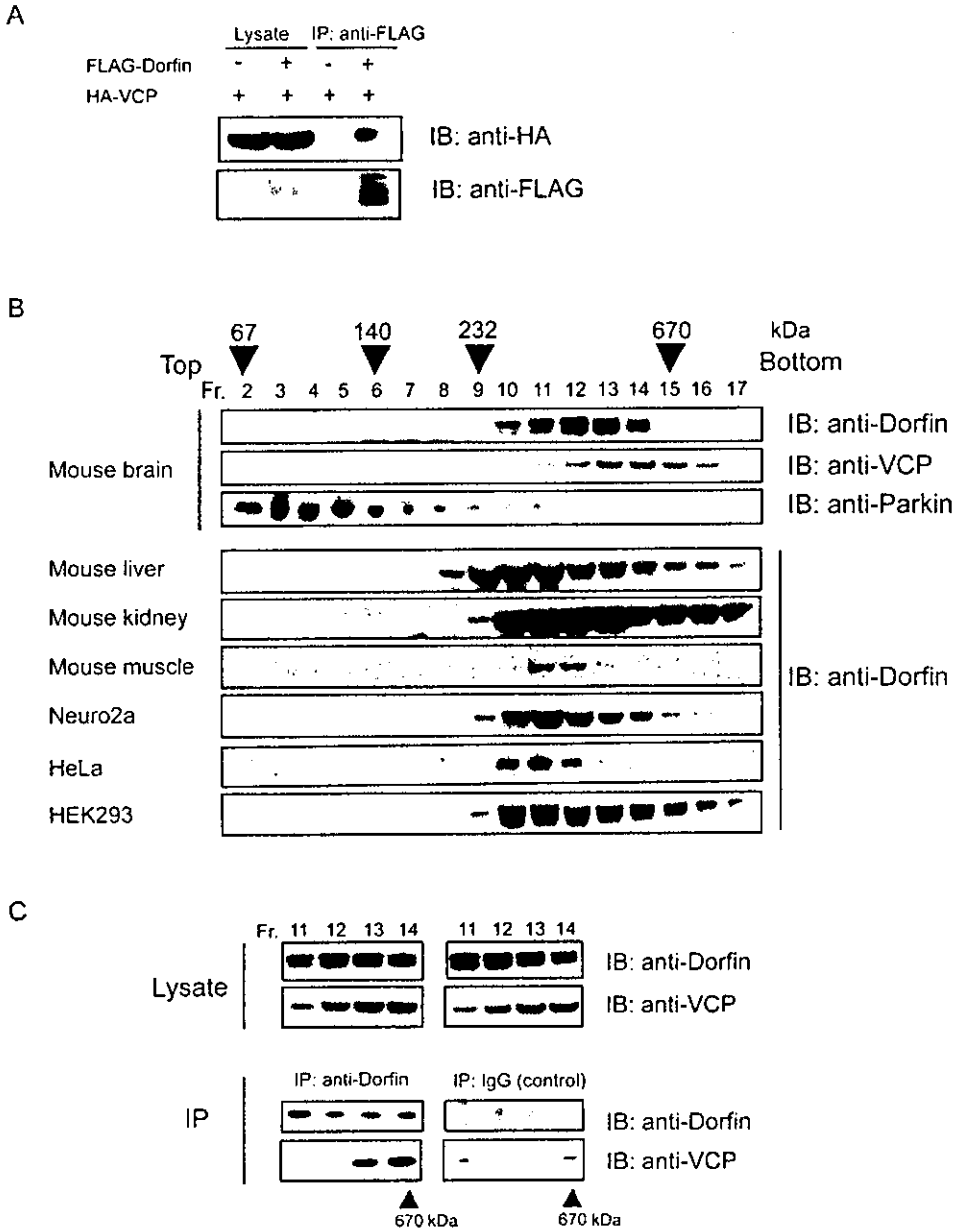


FIG. 1. ***In vivo* interaction between Dorfin and VCP.** *A*, FLAG-Dorfin and HA-VCP are co-expressed in HEK293 cells. FLAG-mock vector was used as a negative control. The amounts of HA-VCP in 10% of the lysate used are shown (*Lysate*); the rest was subjected to immunoprecipitation (*IP*) with anti-FLAG (M2) antibody. Following immunoblotting (*IB*) with anti-HA (12CA5) antibody revealed that HA-VCP was co-immunoprecipitated with FLAG-Dorfin. *B*, 5 mg of protein of various mouse tissues (brain, liver, kidney, and muscle) and 1 mg of protein of cultured cells (HEK293, HeLa, and Neuro2a) were each homogenized in 1 ml of PBS. Supernatants were fractionated by 10–40% glycerol gradient centrifugation followed by separation into 30 fractions using a fraction collector. Immunoblotting using anti-Dorfin, anti-VCP, and anti-Parkin antibodies was performed on the fractions (*Fr.*), including fractions 2–17. Endogenous Dorfin was co-sedimented with VCP in the fractions with a molecular mass of around 400–600 kDa. The positions of co-migrated molecular mass markers are indicated *above* the *panels*. *C*, immunoprecipitation with polyclonal anti-Dorfin antibody (anti-Dorfin-30) was performed on fractions 11–14 collected by glycerol gradient centrifugation analysis, where endogenous Dorfin was seen in *B*. As a negative control, immunoprecipitation with nonimmune rabbit IgG was used on the same fractions.

ble staining of identical sections was performed as described previously (7). In immunofluorescence microscopy, Alexa-488- and Alexa-546-conjugated secondary antibodies (Molecular Probes) were used. All human and animal studies described in this report were approved by the appropriate Ethics Review Committees of the Nagoya University Graduate School of Medicine.

## RESULTS

*Identification of Dorfin-associated Protein in the Cells*—In an effort to identify protein(s) that physically interacts with Dorfin in the cells, FLAG-Dorfin was expressed in HEK293 cells and then immunoprecipitated by anti-FLAG antibody. The immunoprecipitates were eluted with a FLAG peptide and then digested with Lys-C endopeptidase (*Achromobacter* protease I), and the cleaved fragments were directly analyzed using a highly sensitive "direct nanoflow LC-MS/MS" system as described under "Materials and Methods." Following data base search, a total of 13 peptides were assigned to MS/MS spectra obtained from the LC-MS/MS analyses for the FLAG-Dorfin-

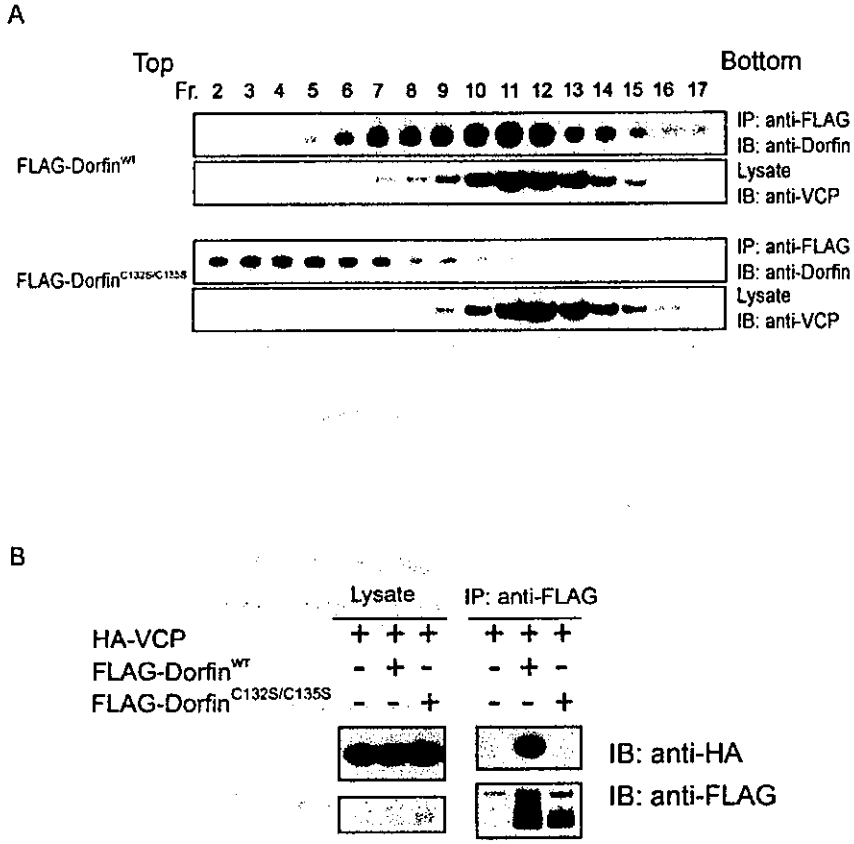


FIG. 2. **Loss of physical interaction between Dorfin$^{C132S/C135S}$ and VCP.** *A*, transfected Dorfin$^{WT}$, but not Dorfin$^{C132S/C135S}$ (*Dorfin$^{C132S-C135S}$*), forms a high $M_r$ complex. Lysate of HEK293 cells overexpressed with FLAG-Dorfin$^{WT}$ or FLAG-Dorfin$^{C132S/C135S}$ was fractionated by 10–40% glycerol gradient centrifugation. The selected fractions (*Fr.*), fractions 2–17, were subjected to immunoprecipitation (*IP*) using anti-FLAG (M2) antibody. Immunoblotting (*IB*) with anti-Dorfin antibody revealed that exogenous FLAG-Dorfin$^{WT}$ formed a high molecular weight complex, whose peak was at fraction 11, whereas FLAG-Dorfin$^{C132S/C135S}$ migrated in fractions of smaller $M_r$ (around fraction 7). Ten percent of the fractionated samples were shown as "lysate." *B*, Dorfin$^{WT}$ can interact with VCP, but Dorfin$^{C132S/C135S}$ cannot. FLAG-Dorfin$^{WT}$ or FLAG-Dorfin$^{C132S/C135S}$ and HA-VCP were co-expressed in HEK293 cells. FLAG-mock vector was used as a negative control. The amounts of HA-VCP in 10% of the lysate used are shown (*Lysate*); the rest was subjected to immunoprecipitation with anti-FLAG (M2) antibody. Following immunoblotting with anti-HA (12CA5) antibody revealed that HA-VCP was co-immunoprecipitated with FLAG-Dorfin$^{WT}$ but not with FLAG-Dorfin$^{C132S/C135S}$.

associated complexes. These peptide data identified nine proteins as candidates for Dorfin-associated proteins. One of these identified proteins was VCP that has been proposed to have multiple functions, such as membrane fusion or endoplasmic reticulum-associated degradation (ERAD) (18–22). In the next step, we examined the relationship between Dorfin and VCP, because the latter has been reported to be linked to various aspects of neurodegeneration (15).

*Dorfin Interacts with VCP in Vivo*—To verify the interaction between Dorfin and VCP, FLAG-Dorfin and HA-VCP were transiently overexpressed in HEK 293 cells. Immunological analyses revealed that HA-VCP was co-immunoprecipitated with FLAG-Dorfin but not with FLAG-mock (Fig. 1*A*), confirming their physical interactions in the cells. To determine whether endogenous Dorfin forms a complex, the lysate from mouse brain homogenate was fractioned by glycerol density gradient centrifugation. Each fraction was immunoblotted with anti-Dorfin antibody. The majority of endogenous Dorfin was co-sedimented with VCP around a size of 400–600 kDa, although endogenous Parkin, which is another RING-IBR type E3 ligase (12), existed in the fractions of much lighter molecular weight ($M_r$) (Fig. 1*B*, *top panels*). Moreover, Dorfin was sedimented in the fractions of 400–600 kDa in other tissues, such as the liver, kidney, and muscle of mouse, and various cultured cells including Neuro2a, HeLa, and HEK293 cells (Fig. 1*B*, *bottom panels*). To determine whether endogenous Dorfin interacts with VCP, immunoprecipitation using polyclonal anti-Dorfin antibody (Dorfin-30) was performed on the fractions shown in Fig. 1*B*, *top panels*. Endogenous VCP was co-immunoprecipitated with endogenous Dorfin in the fractions of high $M_r$ (fractions (*Fr.*) 13 and 14). No apparent band was observed when precipitated with rabbit IgG (Fig. 1*C*).

*Mutations of RING Finger Domain of Dorfin Results in Loss of Dorfin-VCP Interactions*—Next, we examined whether transfected Dorfin (FLAG-Dorfin$^{WT}$) and its RING mutant (FLAG-Dorfin$^{C132S/C135S}$), in which the two Cys residues at positions 132 and 135 within the RING finger domain were substituted for Ser residues, form a complex. The results showed overexpression of FLAG-Dorfin$^{WT}$ in high molecular fractions (*Fr.* in Fig. 2), whose peak was between fractions 10 and 12, whereas overexpressed FLAG-Dorfin$^{C132S/C135S}$ did not consist of high molecular weight complex. Overexpression of FLAG-Dorfin$^{WT}$ or FLAG-Dorfin$^{C132S/C135S}$ did not change the sedimentation pattern of VCP (Fig. 2*A*). Furthermore, immunoprecipitation analysis showed that FLAG-Dorfin$^{WT}$, but not FLAG-Dorfin$^{C132S/C135S}$, could interact with HA-VCP in HEK293 cells (Fig. 2*B*).

*Dorfin Interacts with VCP in Vitro*—To confirm the direct

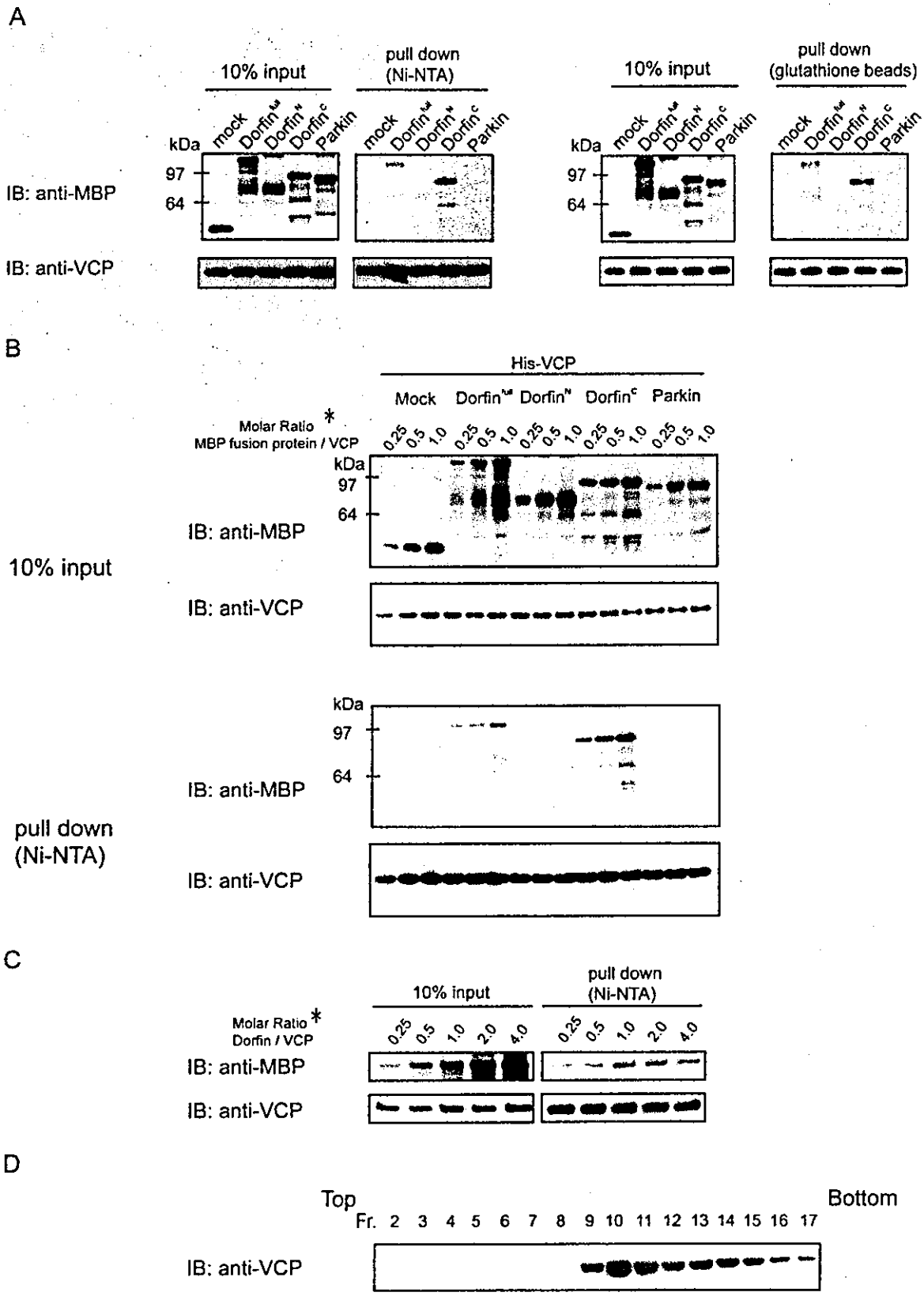


FIG. 3. ***In vitro* interaction between Dorfin and VCP.** *A*, recombinant His- or GST-VCP protein was incubated with MBP-mock, MBP-Dorfin$^{full}$, MBP-Dorfin$^{N}$, MBP-Dorfin$^{C}$, and MBP-Parkin proteins *in vitro*. Two $\mu$g of His- or GST-VCP proteins and MBP fusion proteins at similar molar concentrations to VCP proteins were used for the assays. The amounts of MBP fusion and GST fusion Dorfin derivatives and His-VCP in 10% of the samples used are shown (*10% input*). *NTA*, nitrilotriacetic acid. *IB*, immunoblot. *B*, 2 $\mu$g of His-VCP was incubated with MBP-mock,

binding between Dorfin and VCP and to determine the exact portion of Dorfin that interacts with VCP *in vitro*, we performed pull-down assays using recombinant proteins. Recombinant MBP-Dorfin or its deletion mutants (*i.e.* MBP-Dorfin$^{N}$ and MBP-Dorfin$^{C}$) and the same molar of recombinant His-VCP or GST-VCP were mixed and incubated for 1 h at 4 °C. MBP-mock protein was used as a negative control in these experiments. A small portion of MBP-Dorfin$^{full}$ or Dorfin$^{C}$ (C-terminal substrate-recognizing domain) bound to both His-VCP and GST-VCP, whereas MBP-mock, MBP-Dorfin$^{N}$ (N-terminal RING-IBR domain), and MBP-Parkin did not bind to His-VCP or GST-VCP (Fig. 3*A*). We next determined the number of Dorfins that bind one hexamer of VCP. To investigate this issue, we incubated His-VCP with increasing amounts of MBP-Dorfin$^{full}$, MBP-Dorfin$^{N}$, MBP-Dorfin$^{C}$, MBP-mock, or MBP-Parkin. As shown in Fig. 3*B*, the amount of binding portion of MBP-Dorfin$^{full}$ and -Dorfin$^{C}$ pulled down with His-VCP was not saturated below the even molar ratio. The pull-down experiments using excess amounts of MBP-Dorfin$^{full}$ revealed that MBP-Dorfin$^{full}$ was saturated at the even molar ratio (Fig. 3*C*). As reported previously (15), recombinant His-VCP sedimented in high molecular weight fractions, indicating that it formed a hexamer *in vitro* (Fig. 3*D*). These findings indicated that six Dorfin molecules were likely bind to a VCP complex *in vitro*.

*Subcellular Localization of Dorfin and VCP in HEK293 Cells*—In previous studies, we showed that exogenous and endogenous Dorfin resided perinuclearly and was colocalized with Vimentin in cultured cells treated with a proteasome inhibitor (4). The staining patterns of Dorfin were indistinguishable from those of the aggresome, namely a pericentriolar, membrane-free, cytoplasmic inclusion containing misfolded ubiquitylated proteins packed in a cage of intermediate filaments (4). VCP immunostaining was also observed throughout aggresomes in cultured neuronal cells when induced by treatment with a proteasome inhibitor (15). In order to examine the subcellular localization of Dorfin and VCP, GFP-Dorfin and HA-VCP were co-expressed in HEK293 cells. Without proteasome treatment, GFP-Dorfin-expressing cells showed granular fluorescence in the cytosol, and the HA-VCP-expressing cells showed diffuse and uniform cytoplasmic staining (Fig. 4*A*). Treatment with MG132 (1 μM, 16 h) resulted in accumulation of both GFP-Dorfin and HA-VCP and perinuclear colocalization as a clear large protein aggregate that mimics aggresomes (Fig. 4*B*).

*Colocalization of Dorfin and VCP in the Affected Neurons of ALS and PD*—In previous studies, immunostaining of Dorfin and VCP was independently noted in LBs of PD, and the peripheral staining pattern of both proteins in LBs was similar (7, 23). To confirm the immunoreactivities of Dorfin and VCP in the affected neurons in ALS and PD, we performed a double-labeling immunofluorescence study using a rabbit polyclonal anti-Dorfin antibody (Dorfin-41) and a mouse monoclonal VCP antibody on the postmortem samples of ALS and PD. In the ALS spinal cords, both proteins were colocalized in the LB-like inclusions (Fig. 5, *A–F*). The margin of LBs in PD was intensely immunostained for Dorfin and VCP, and merged images confirmed their strong colocalization (Fig. 5, *G–L*). Dorfin and VCP were also positive in Lewy neurites in the affected neurons of PD (Fig. 5, *M–O*).

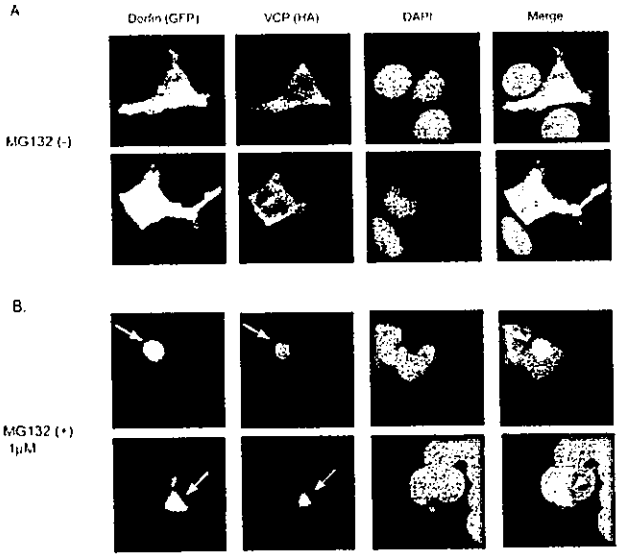


FIG. 4. **Subcellular localization of GFP-Dorfin and HA-VCP in HEK293 cells treated or untreated with a proteasome inhibitor.** GFP-Dorfin and HA-VCP were co-expressed transiently in HEK 293 cells. Cells were treated with (*B*) or without (*A*) 1 μM MG132 for 16 h. HA-VCP was stained with anti-monoclonal HA antibody (12CA5). Nuclei were stained with 4′,6-diamidino-2-phenylindole (*DAPI*). Without the treatment of MG132, GFP-Dorfin was spread through the cytosol, and it appeared like small aggregations. HA-VCP was also seen mainly in the cytosol and partly colocalized with GFP-Dorfin (*A*). After treatment with 1 μM MG132 for 16 h, both GFP-Dorfin and HA-VCP showed perinuclear accumulation and colocalization and appeared as clear large protein aggregates (*B*; *arrows*).

*Dorfin Ubiquitylates Mutant SOD1 in Vivo*—Unlike the wild-type form, mutant SOD1 proteins are rapidly degraded by the ubiquitin-proteasome system. Consistent with our previous results (5), SOD1$^{G93A}$ and SOD1$^{G85R}$ were polyubiquitylated, and co-expression with FLAG-Dorfin$^{WT}$ enhanced polyubiquitylation of these mutant SOD1s compared with co-expression with FLAG-BAP, a negative control construct (Fig. 6*A*). Boiling with 1% SDS-containing buffer did not change the level of ubiquitylated mutant SOD1, indicating that mutant SOD1 itself was ubiquitylated by Dorfin (Fig. 6*B*). We also performed the same *in vivo* ubiquitylation assay using Neuro2a cells to examine for E3 activity of Dorfin in neuronal cells. The enhanced polyubiquitylation of these mutant SOD1s by Dorfin was observed in Neuro2a cells as well as in HEK293 cells (Fig. 6*C*). FLAG-Dorfin$^{C132S/C135S}$ did not enhance polyubiquitylation of mutant SOD1s, indicating that this RING finger mutant form was functionally inactive (Fig. 6*D*).

*VCP$^{K524A}$ Suppresses the E3 Activity of Dorfin*—VCP has two ATPase binding domains (D1 and D2). A D2 domain mutant, VCP$^{K524A}$, induces cytoplasmic vacuoles, which mimics vacuole formation seen in the affected neurons in various neurodegenerative diseases (11, 15). The D2 domain represents the major ATPase activity and is essential for VCP function (11). The ATPase activity of VCP$^{K524A}$ is much lower than that of VCP$^{WT}$, and VCP$^{K524A}$ caused accumulation of polyubiquitylated proteins in the nuclear and membrane fractions together with elevation of ER stress marker proteins due to ERAD

MBP-Dorfin$^{full}$, MBP-Dorfin$^{N}$, MBP-Dorfin$^{C}$, and MBP-Parkin with increasing amounts (molar ratio to VCP: 0.25, 0.5, and 1.0). The amounts of MBP fusion Dorfin derivatives and His-VCP in 10% of the samples used are shown (10% input). *C*, 2 μg of His-VCP was incubated with MBP-Dorfin$^{full}$ with increasing amounts (molar ratio to VCP: 0.25, 0.5, 1, 2, and 4). The amounts of MBP-Dorfin$^{full}$ and His-VCP in 10% of the samples used are shown (*10% input*). *D*, His-VCP protein (0.5 μg) was fractionated by 10–40% glycerol gradient centrifugation followed by separation into 30 fractions using a fraction collector. Immunoblotting using anti-VCP antibody was performed on the selected fractions (fractions 2–17). *, The molar ratio was calculated by the amount of VCP monomers, not VCP complexes.

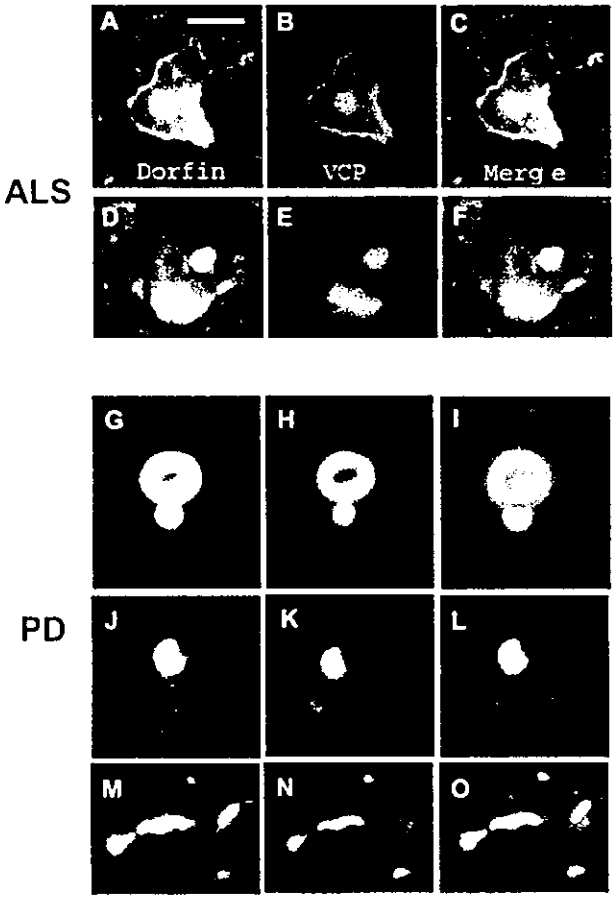


FIG. 5. **Colocalization of Dorfin-41 immunoreactivity with VCP in neuronal inclusions in ALS and PD.** Sections were doubly labeled with anti-Dorfin-41 antiserum and monoclonal VCP antibody and analyzed with a laser-scanning confocal microscope. The *left panels* (*green*) correspond to Dorfin, *middle panels* (*red*) correspond to VCP, and *right panels* correspond to merged images; structures in *yellow* indicate colocalization. Colocalization of Dorfin and VCP is seen in LB-like inclusions in motor neurons of the spinal cord of ALS (*A–F*). Dorfin is also colocalized with VCP in the margin of LBs (*G–I*), premature LBs (*J–L*), and Lewy neurites (*M–O*) in the nigral neurons of PD. *Scale bars*, 20 μm (*A–L*) and 10 μm (*M–O*).

inhibition, whereas its expression level, localization, and complex formation were indistinguishable from those of $VCP^{WT}$ (11). In order to examine the functional effect of VCP on Dorfin, $VCP^{WT}$, $VCP^{K524A}$, or LacZ was co-expressed with $SOD1^{G85R}$, FLAG-Dorfin, and HA-Ub in HEK293 cells. Co-expression with $VCP^{K524A}$ showed a marked decline of polyubiquitylation of $SOD1^{G85R}$ compared with co-expression with $VCP^{WT}$ or LacZ (Fig. 7*A*, *top* and *middle*). Since Dorfin physically interacts with mutant SOD1s (5), we next investigated whether this decline of polyubiquitylation of $SOD1^{G85R}$ was mediated by reduced affinity between $SOD1^{G85R}$ and Dorfin. Immunoprecipitation by anti-FLAG antibody showed that $VCP^{K524A}$ did not change affinity between $SOD1^{G85R}$ and Dorfin (Fig. 7*A*, *bottom*). Neither $VCP^{WT}$ nor $VCP^{K524A}$ changed the level of polyubiquitylation protein in the total lysate (Fig. 7*B*). To clarify whether this negative effect of $VCP^{K524A}$ is specific for Dorfin, we assessed the autoubiquitylation of FLAG-Parkin in the presence of $VCP^{WT}$, $VCP^{K524A}$, or LacZ. Co-expression of $VCP^{K524A}$ did not decrease autoubiquitylation of FLAG-Parkin compared with co-expression of LacZ or $VCP^{WT}$ (Fig. 7*C*). We performed the same experiments using Neuro2a cells to see whether $VCP^{K524A}$ suppress the E3 activity of Dorfin in neuronal cells. The marked decline of polyubiquitylation of $SOD1^{G85R}$ by $VCP^{K524A}$ expression was also seen in Neuro2a cells (Fig. 7*D*).

## DISCUSSION

UBIs in the affected neurons are histopathological hallmarks in various neurodegenerative disorders (8). Dorfin is an E3 ligase, which can ubiquitylate mutant SOD1s and synphilin-1 (5, 24). These substrates and Dorfin were identified in UBIs in various neurodegenerative diseases, such as LB-like inclusions in ALS and LBs in PD and dementia with Lewy bodies (7). This finding suggests that Dorfin may play a crucial role in the process of generating inclusions in the affected neurons. In the present study, we identified VCP as one of the Dorfin-associated proteins using mass spectrometry, and VCP-Dorfin physical interaction was confirmed by an immunoprecipitation experiment using FLAG-Dorfin and HA-VCP overexpressed in HEK293 cells (Fig. 1*A*). VCP is an essential and highly conserved protein of the AAA-ATPase family, which is considered to have diverse cellular functions, such as membrane fusion (25–27), nuclear trafficking (28), cell proliferation (29, 30), and the ERAD pathway (18–22). Many reports have implied that VCP is involved in the pathogenesis of various neuromuscular diseases. VCP has been implicated as a factor that modifies the progress of polyglutamine-induced neuronal cell death (15). In addition, histopathological studies revealed positive staining for VCP in UBIs in PD and ALS with dementia (23). VCP is also associated with MJD protein/atxin-3, in which abnormal expansion of polyglutamine tracts causes Machado-Joseph disease/spinocerebellar ataxia type 3 (31). VCP is also required for the degradation of ataxin-3 in collaboration with E4B/Ufd2a, a ubiquitin chain assembly factor (E4) (32). Recent studies have indicated that missense mutations in the VCP gene cause inclusion body myopathy associated with Paget's disease of bone and frontotemporal dementia, which is characterized by the presence of vacuoles in the cytoplasm in muscle fibers (33).

Our results showed that endogenous Dorfin formed a 400–600-kDa complex in various tissues and various cultured cells (Fig. 1*B*). Dorfin is a ~91-kDa protein; therefore, this high $M_r$ complex should include Dorfin-associated proteins, although the possibility that Dorfin itself oligomerizes in the cell cannot be excluded. Glycerol gradient centrifugation analysis and immunoprecipitation experiments in the present study showed that endogenous Dorfin interacted with endogenous VCP in a complex of approximately 600 kDa, possibly including a Dorfin molecule and a hexametric form of VCP (Fig. 1*C*).

The first RING mutant of Dorfin, in which Cys at positions 132 and 135 changed to Ser, was prepared. This mutant Dorfin, $Dorfin^{C132S/C135S}$, could not ubiquitylate mutant SOD1s (Fig. 6*D*). Glycerol gradient centrifugation analysis revealed that $Dorfin^{C132S/C135S}$ did not form a high $M_r$ complex, whereas exogenous wild type Dorfin ($Dorfin^{WT}$) formed a high $M_r$ complex similar to endogenous Dorfin (Fig. 2*A*). Furthermore, an immunoprecipitation experiment using $Dorfin^{WT}$ and $Dorfin^{C132S/C135S}$ revealed that $Dorfin^{WT}$ could interact with VCP, whereas $Dorfin^{C132S/C135S}$ could not (Fig. 2*B*).

Our *in vitro* study using recombinant proteins showed that full-length ($MBP\text{-}Dorfin^{full}$) and the C terminus of Dorfin ($MBP\text{-}Dorfin^{C}$) directly interacted with VCP, whereas the $MBP\text{-}Dorfin^{N}$ mutant, containing the entire RING finger domain (amino acid residues 1–367), did not bind to VCP (Fig. 3*A*). This finding was unexpected, since *in vivo* binding analysis suggested that Dorfin could interact with VCP at the RING finger domain. It is plausible that certain structural changes in $Dorfin^{C132S/C135S}$ might render the C-terminal VCP-binding portion incapable of accessing VCP molecules. This may explain the result that $Dorfin^{C132S/C135S}$ did not form a high $M_r$ complex.

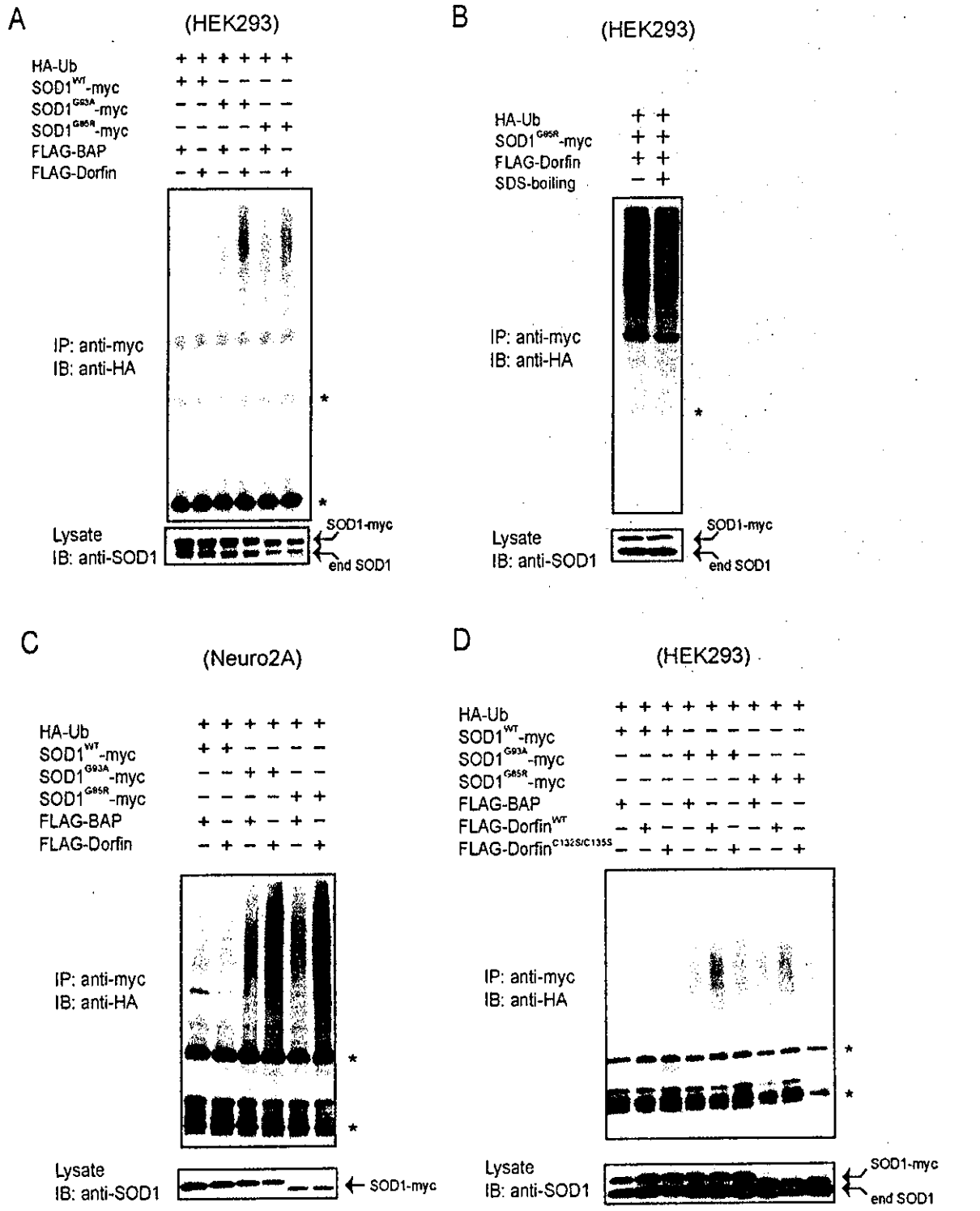


FIG. 6. **Dorfin ubiquitylates mutant SOD1s *in vivo*.** *A*, increased ubiquitylation of mutant SOD1 proteins by overexpression of Dorfin. HEK293 cells were co-transfected with $SOD1^{WT}$-Myc, $SOD1^{G93A}$-Myc, or $SOD1^{G85R}$-Myc and HA-Ub with or without FLAG-Dorfin. FLAG-bovine alkaline phosphatase (*BAP*) was used as a negative control. Immunoprecipitation (*IP*) was performed with Myc antibody (9E10). *IB*, immunoblotting. *B*, SDS boiling was performed prior to immunoprecipitation. To examine covalently ubiquitylated molecules, the cell lysate was boiled with the buffer containing 1% SDS for 5 min. Immunoprecipitation with Myc antibody (9E10) showed that the SDS-boiling procedure did not change polyubiquitylation level of $SOD1^{G85R}$-Myc by Dorfin. *C*, increased ubiquitylation of mutant SOD1 proteins by overexpression of Dorfin in Neuro2a cells. The same *in vivo* ubiquitylation assay as in *A* was performed using Neuro2a cells. *D*, $Dorfin^{C132S/C135S}$ ($Dorfin^{C132S/C135S}$) did not have E3 activity on mutant SOD1. HEK293 cells were co-transfected with $SOD1^{WT}$-Myc, $SOD1^{G93A}$-Myc, or $SOD1^{G85R}$-Myc and HA-Ub with FLAG-$Dorfin^{WT}$ or FLAG-$Dorfin^{C132S/C135S}$. The *asterisks* indicate IgG light and heavy chains.

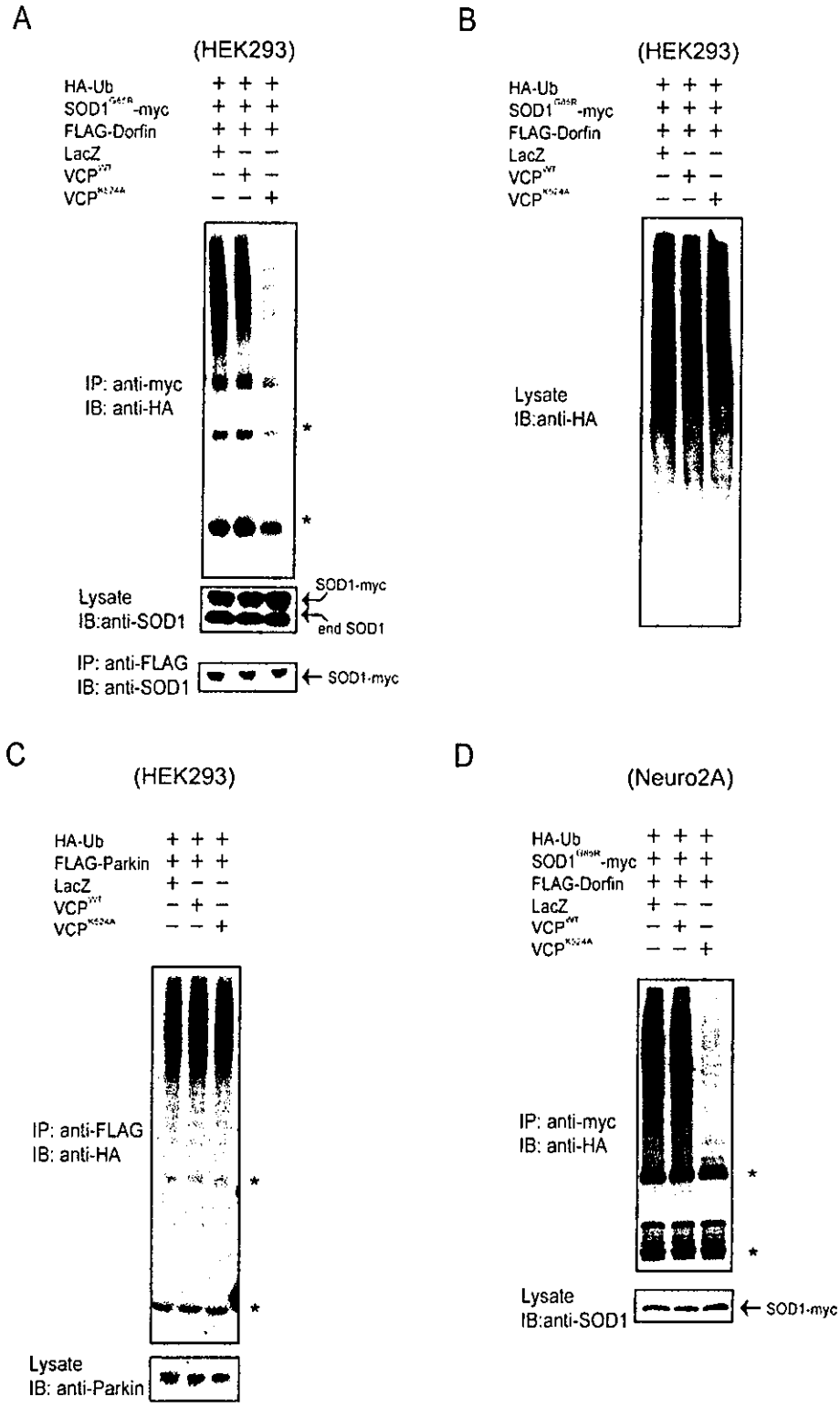


FIG. 7. **A dominant negative mutant of VCP, VCP$^{K524A}$ inhibits the E3 ubiquitin ligase activity of Dorfin.** *A*, inhibition of dominant negative form mutant VCP$^{K524A}$ on the E3 ubiquitin ligase activity of Dorfin. HEK293 cells were co-transfected with SOD1$^{G85R}$-Myc, HA-Ub, FLAG-Dorfin, and VCP$^{WT}$, VCP$^{K524A}$, or LacZ. Immunoprecipitation (*IP*) was performed with Myc antibody (9E10) and FLAG antibody (M2). *IB*, immunoblotting. *B*, neither VCP$^{WT}$ nor VCP$^{K524A}$ changed the level of total polyubiquitylated protein in the cell lysate. Ten percent of the volume of HEK293 cells used in *A* was subjected to immunoblotting using anti-HA (12CA5) antibody. *C*, autoubiquitylation of FLAG-Parkin was not influenced by the dominant negative form VCP$^{K524A}$. HEK293 cells were co-transfected with FLAG-Parkin, HA-Ub, and VCP$^{WT}$, VCP$^{K524A}$, or LacZ. Immunoprecipitation with FLAG antibody (M2) was performed. *D*, inhibition of VCP$^{K524A}$ on E3 ubiquitin ligase activity of Dorfin in Neuro2a cells. Neuro2a cells were co-transfected with SOD1$^{G85R}$-Myc, HA-Ub, FLAG-Dorfin, and VCP$^{WT}$, VCP$^{K524A}$, or LacZ. Immunoprecipitation was performed using Myc antibody (9E10) and FLAG antibody (M2). The *asterisks* indicate IgG light and heavy chains.

The amount of Dorfin bound with VCP was saturated at even molar ratio *in vitro* (Fig. 3, *B* and *C*). Since VCP exists as a homohexamer (Fig. 3*D*), the *in vivo* observed size of ~600 kDa appears to be too small for the Dorfin-VCP complex if one VCP molecule binds to more than one Dorfin as shown in *in vitro* experiments. However, it is noteworthy that the size of molecules estimated by glycerol density gradient centrifugation analysis used in this study is not accurate and sufficient to discuss the molecular interaction of Dorfin and VCP in the cells. To date, various adaptor proteins, with which VCP forms multiprotein complexes, have been identified, such as Npl4, Ufd1 (18, 20), Ufd2 (34), Ufd3 (35), p47 (36), or SVIP (37). Although our *in vitro* study showed direct physical interaction between Dorfin and VCP, the environment with those adaptor proteins might reflect *in vivo* conditions. This also may explain the apparent discrepancy of the Dorfin-VCP binding fashions between *in vivo* and *in vitro* analyses.

Treatment with a proteasomal inhibitor causes the translocation of endogenous VCP and Dorfin to the aggresome in cultured cells (4, 15). Our results showed that these two proteins indeed colocalized perinuclearly in the aggresome following treatment with a proteasomal inhibitor (Fig. 4). Furthermore, we were able to demonstrate both Dorfin and VCP immunoreactivities in LB-like inclusions in ALS and LBs in PD (Fig. 5). In the majority of LBs, indistinguishable peripheral staining patterns were observed with both anti-Dorfin and anti-VCP antibodies. These results confirmed that both Dorfin and VCP are associated with the formation processes of aggresomes and inclusion bodies through physical interaction.

We showed here that co-expression of $VCP^{K524A}$ resulted in a marked decrease of ubiquitylation activity of Dorfin compared with co-expression of $VCP^{WT}$ or control. On the other hand, $VCP^{K524A}$ failed to decrease autoubiquitylation activity of Parkin. $VCP^{K524A}$ did not change the level of polyubiquitylated protein accumulation in the cell lysate in this study (Fig. 7). Knockdown experiments using the RNA interference technique showed accumulation of polyubiquitylated proteins (38). Combined with the observation that inhibition of VCP did not decrease the general accumulation of polyubiquitylated proteins, our results indicated that the E3 regulation function of VCP may be specific to certain E3 ubiquitin ligases such as Dorfin. VCP is an abundant protein that accounts for more than 1% of protein in the cell cytosol and is known to have various chaperone-like activities (39); therefore, it may function as a scaffold protein on the E3 activity of Dorfin. The localization of Dorfin and VCP in UBIs in various neurodegenerative disorders indicates the involvement of these proteins in the quality control system for abnormal proteins accumulated in the affected neurons in neurodegenerative disorders.

Since the unfolded protein response and ERAD are dynamic responses required for the coordinated disposal of misfolded proteins (40), the ERAD pathway can be critical for the etiology of neuronal cell death caused by various unfolded proteins. VCP is required for multiple aspects of the ERAD system by recognition of polyubiquitylated proteins and translocations to the 26 S proteasome for processive degradation through the VCP-Npl4-Ufd1 complex (18, 41). Our results suggest the involvement of Dorfin in the ERAD system, which is related to the pathogenesis of neurodegenerative disorders, such as PD or Alzheimer's disease. Further study including Dorfin knockout and/or knockdown models should examine the pathophysiology of Dorfin in association with the ERAD pathway or other cellular functions. Such studies should enhance our understanding of the pathogenetic role of Dorfin in neurodegenerative disorders.

REFERENCES


1. Julien, J. P. (2001) *Cell* **104**, 581–591
2. Rowland, L. P., and Shneider, N. A. (2001) *N. Engl. J. Med.* **344**, 1688–1700
3. Ishigaki, S., Niwa, J., Ando, Y., Yoshihara, T., Sawada, K., Doyu, M., Yamamoto, M., Kato, K., Yotsumoto, Y., and Sobue, G. (2002) *FEBS Lett.* **531**, 354–358
4. Niwa, J., Ishigaki, S., Doyu, M., Suzuki, T., Tanaka, K., and Sobue, G. (2001) *Biochem. Biophys. Res. Commun.* **281**, 706–713
5. Niwa, J., Ishigaki, S., Hishikawa, N., Yamamoto, M., Doyu, M., Murata, S., Tanaka, K., Taniguchi, N., and Sobue, G. (2002) *J. Biol. Chem.* **277**, 36793–36798
6. Ciechanover, A., and Brundin, P. (2003) *Neuron* **40**, 427–446
7. Hishikawa, N., Niwa, J., Doyu, M., Ito, T., Ishigaki, S., Hashizume, Y., and Sobue, G. (2003) *Am. J. Pathol.* **163**, 609–619
8. Mayer, R. J., Lowe, J., Lennox, G., Doherty, F., and Landon, M. (1989) *Prog. Clin. Biol. Res.* **317**, 809–818
9. Johnston, J. A., Ward, C. L., and Kopito, R. R. (1998) *J. Cell Biol.* **143**, 1883–1898
10. Kopito, R. R. (2000) *Trends Cell Biol.* **10**, 524–530
11. Kobayashi, T., Tanaka, K., Inoue, K., and Kakizuka, A. (2002) *J. Biol. Chem.* **277**, 47358–47365
12. Shimura, H., Hattori, N., Kubo, S., Mizuno, Y., Asakawa, S., Minoshima, S., Shimizu, N., Iwai, K., Chiba, T., Tanaka, K., and Suzuki, T. (2000) *Nat. Genet.* **25**, 302–305
13. Fukuchi, M., Imamura, T., Chiba, T., Ebisawa, T., Kawabata, M., Tanaka, K., and Miyazono, K. (2001) *Mol. Biol. Cell* **12**, 1431–1443
14. Ishigaki, S., Liang, Y., Yamamoto, M., Niwa, J., Ando, Y., Yoshihara, T., Takeuchi, H., Doyu, M., and Sobue, G. (2002) *J. Neurochem.* **82**, 576–584
15. Hirabayashi, M., Inoue, K., Tanaka, K., Nakadate, K., Ohsawa, Y., Kamei, Y., Popiel, A. H., Sinohara, A., Iwamatsu, A., Kimura, Y., Uchiyama, Y., Hori, S., and Kakizuka, A. (2001) *Cell Death Differ.* **8**, 977–984
16. Natsume, T., Yamauchi, Y., Nakayama, H., Shinkawa, T., Yanagida, M., Takahashi, N., and Isobe, T. (2002) *Anal. Chem.* **74**, 4725–4733
17. Matsuda, N., Suzuki, T., Tanaka, K., and Nakano, A. (2001) *J. Cell Sci.* **114**, 1949–1957
18. Bays, N. W., and Hampton, R. Y. (2002) *Curr. Biol.* **12**, R366–R371
19. Ye, Y., Meyer, H. H., and Rapoport, T. A. (2001) *Nature* **414**, 652–656
20. Braun, S., Matuschewski, K., Rape, M., Thoms, S., and Jentsch, S. (2002) *EMBO J.* **21**, 615–621
21. Jarosch, E., Taxis, C., Volkwein, C., Bordallo, J., Finley, D., Wolf, D. H., and Sommer, T. (2002) *Nat. Cell Biol.* **4**, 134–139
22. Rabinovich, E., Kerem, A., Frohlich, K. U., Diamant, N., and Bar-Nun, S. (2002) *Mol. Cell. Biol.* **22**, 626–634
23. Mizuno, Y., Hori, S., Kakizuka, A., and Okamoto, K. (2003) *Neurosci. Lett.* **343**, 77–80
24. Ito, T., Niwa, J., Hishikawa, N., Ishigaki, S., Doyu, M., and Sobue, G. (2003) *J. Biol. Chem.* **278**, 29106–29114
25. Meyer, H. H., Kondo, H., and Warren, G. (1998) *FEBS Lett.* **437**, 255–257
26. Kondo, H., Rabouille, C., Newman, R., Levine, T. P., Pappin, D., Freemont, P., and Warren, G. (1997) *Nature* **388**, 75–78
27. Rabouille, C., Kondo, H., Newman, R., Hui, N., Freemont, P., and Warren, G. (1998) *Cell* **92**, 603–610
28. Hetzer, M., Meyer, H. H., Walther, T. C., Bilbao-Cortes, D., Warren, G., and Mattaj, I. W. (2001) *Nat. Cell Biol.* **3**, 1086–1091
29. Frohlich, K. U., Fries, H. W., Rudiger, M., Erdmann, R., Botstein, D., and Mecke, D. (1991) *J. Cell Biol.* **114**, 443–453
30. Asai, T., Tomita, Y., Nakatsuka, S., Hoshida, Y., Myoui, A., Yoshikawa, H., and Aozasa, K. (2002) *Jpn. J. Cancer Res.* **93**, 296–304
31. Kawaguchi, Y., Okamoto, T., Taniwaki, M., Aizawa, M., Inoue, M., Katayama, S., Kawakami, H., Nakamura, S., Nishimura, M., Akiguchi, I., Kimura, J., Narumiya, S., and Kakizuka, A. (1994) *Nat. Genet.* **8**, 221–228
32. Matsumoto, M., Yada, M., Hatakeyama, S., Ishimoto, H., Tanimura, T., Tsuji, S., Kakizuka, A., Kitagawa, M., and Nakayama, K. I. (2004) *EMBO J.* **23**, 659–669
33. Watts, G. D., Wymer, J., Kovach, M. J., Mehta, S. G., Mumm, S., Darvish, D., Pestronk, A., Whyte, M. P., and Kimonis, V. E. (2004) *Nat. Genet.* **36**, 377–381
34. Koegl, M., Hoppe, T., Schlenker, S., Ulrich, H. D., Mayer, T. U., and Jentsch, S. (1999) *Cell* **96**, 635–644
35. Ghislain, M., Dohmen, R. J., Levy, F., and Varshavsky, A. (1996) *EMBO J.* **15**, 4884–4899
36. Meyer, H. H., Wang, Y., and Warren, G. (2002) *EMBO J.* **21**, 5645–5652
37. Nagahama, M., Suzuki, M., Hamada, Y., Hatsuzawa, K., Tani, K., Yamamoto, A., and Tagaya, M. (2003) *Mol. Biol. Cell* **14**, 262–273
38. Wojcik, C., Yano, M., and DeMartino, G. N. (2004) *J. Cell Sci.* **117**, 281–292
39. Dalal, S., and Hanson, P. I. (2001) *Cell* **104**, 5–8
40. Travers, K. J., Patil, C. K., Wodicka, L., Lockhart, D. J., Weissman, J. S., and Walter, P. (2000) *Cell* **101**, 249–258
41. Dai, R. M., and Li, C. C. (2001) *Nat. Cell Biol.* **3**, 740–744

DOI: 10.1093/brain/awg012 *Brain* (2003), **126**, 134–151

# Demyelinating and axonal features of Charcot–Marie–Tooth disease with mutations of myelin-related proteins (PMP22, MPZ and Cx32): a clinicopathological study of 205 Japanese patients

Naoki Hattori,[1] Masahiko Yamamoto,[1] Tsuyoshi Yoshihara,[1] Haruki Koike,[1] Masanori Nakagawa,[2] Hiroo Yoshikawa,[3] Akio Ohnishi,[4] Kiyoshi Hayasaka,[5] Osamu Onodera,[6] Masayuki Baba,[7] Hitoshi Yasuda,[8] Toyokazu Saito,[9] Kenji Nakashima,[10] Jun-ichi Kira,[11] Ryuji Kaji,[12] Nobuyuki Oka[13] Gen Sobue[1] and and the Study Group for Hereditary Neuropathy in Japan

[1]*Department of Neurology, Nagoya University Graduate School of Medicine, Nagoya,* [2]*Third Department of Internal Medicine, Kagoshima University Faculty of Medicine, Kagoshima,* [3]*Department of Neurology, Osaka Kosei-Nenkin Hospital, Osaka,* [4]*Department of Neurology, School of Medicine, University of Occupational and Environmental Health, Kitakyushu,* [5]*Department of Pediatrics, Yamagata University School of Medicine, Yamagata,* [6]*Department of Neurology, Niigata University Graduate School of Medicine and Dental Sciences, Niigata,* [7]*Department of Neurology, Hirosaki University School of Medicine, Hirosaki,* [8]*Third Department of Internal Medicine, Shiga University of Medical Science, Otsu,* [9]*Department of Neurology, Kitasato University School of Medicine, Sagamihara,* [10]*Department of Neurology, Tottori University Faculty of Medicine, Yonago,* [11]*Department of Neurology, Kyushu University Graduate School of Medicine, Fukuoka,* [12]*Division of Advanced Clinical Neuroscience, University of Tokushima School of Medicine, Tokushima and* [13]*Department of Internal Medicine, Hyogo College of Medicine, Nishinomiya, Japan*

*Correspondence to: Gen Sobue, MD, Department of Neurology, Nagoya University Graduate School of Medicine, 65 Tsurumai-cho Showa-ku Nagoya 466 8550, Japan*
*E-mail: sobueg@tsuru.med.nagoya-u.ac.jp*

## Summary

**Three genes commonly causing Charcot–Marie–Tooth disease (CMT) encode myelin-related proteins: peripheral myelin protein 22 (PMP22), myelin protein zero (MPZ) and connexin 32 (Cx32). Demyelinating versus axonal phenotypes are major issues in CMT associated with mutations of these genes. We electrophysiologically, pathologically and genetically evaluated demyelinating and axonal features of 205 Japanese patients with PMP22 duplication, MPZ mutations or Cx32 mutations. PMP22 duplication caused mainly demyelinating phenotypes with slowed motor nerve conduction velocity (MCV) and demyelinating histopathology, while axonal features were variably present. Two distinctive phenotypic subgroups were present in patients with MPZ mutations: one showed preserved MCV and exclusively axonal pathological features, while the other was exclusively demyelinating. These axonal and demyelinating phenotypes were well concordant among siblings in individual families, and MPZ mutations did not overlap among these two subgroups, suggesting that the nature and position of the MPZ mutations mainly determine the axonal and demyelinating phenotypes. Patients with Cx32 mutations showed intermediate slowing of MCV, predominantly axonal features and relatively mild demyelinating pathology. These axonal and demyelinating features were present concomitantly in individual patients to a variable extent. The relative severity of axonal and demyelinating features was not associated with**

**particular Cx32 mutations. Median nerve MCV and overall histopathological phenotype changed little with disease advancement. Axonal features of diminished amplitudes of compound muscle action potentials (CMAPs), axonal loss, axonal sprouting and neuropathic muscle wasting all changed as disease advanced, especially in PMP22 duplication and Cx32 mutations. Median nerve MCVs were well maintained independently of age, disease duration and the severity of clinical and pathological abnormalities, confirming that median nerve MCV is an excellent marker for the genetically determined neuropathic phenotypes. Amplitude of CMAPs was correlated significantly with distal muscle strength in PMP22 duplication, MPZ mutations and Cx32 mutations, while MCV slowing was not, indicating that clinical weakness results from reduced numbers of functional large axons, not from demyelination. Thus, the three major myelin-related protein mutations induced varied degrees of axonal and demyelinating phenotypic features according to the specific gene mutation as well as the stage of disease advancement, while clinically evident muscle wasting was attributable to loss of functioning large axons.**

**Keywords:** Charcot–Marie–Tooth disease; PMP22; MPZ; Cx32

**Abbreviations:** CK = creatine kinase; CMAP = compound muscle action potential; CMT = Charcot–Marie–Tooth disease; Cx32 = connexin 32; DL = distal latency; MCV = motor nerve conduction velocity; MPZ = myelin protein zero; PMP22 = peripheral myelin protein 22; SCV = sensory nerve conduction velocity; SNAP = sensory nerve action potential

## Introduction

Charcot–Marie–Tooth disease (CMT) refers to a pathologically and genetically heterogeneous group of motor and sensory neuropathies characterized by slowly progressive weakness, muscle atrophy and sensory impairment, all most marked in the distal part of the legs. Two major phenotypes have been distinguished (Dyck and Lambert, 1968; Buchthal and Behse, 1977; Harding and Thomas, 1980). Type 1 (CMT1), the demyelinating form of CMT, results in a marked decrease in nerve conduction velocity (NCV) and segmental demyelination of peripheral nerves; type 2 (CMT2), the axonal form of CMT, shows primarily axonal involvement, with normal or slightly decreased NCV, as well as nerve fibre loss and axonal sprouting. In addition, a group showing features intermediate between those of types 1 and 2 has also been described (Bradley *et al.*, 1977). Many causative genes have been identified, prompting proposals for a new classification (Harding, 1995; Kamholz *et al.*, 2000; Reilly, 2000). Heterozygous duplication of the locus for the peripheral nerve myelin protein 22 (PMP22) gene on chromosome 17p11.2 is found in most patients with demyelinating CMT1A (Lupski *et al.*, 1991; Raeymaekers *et al.*, 1991; Matsunami *et al.*, 1992; Patel *et al.*, 1992; Timmerman *et al.*, 1992). Occasionally, a point mutation in the PMP22 gene rather than duplication is found in CMT1A patients (Nelis *et al.*, 1996; Kovach *et al.*, 1999). CMT1B, another demyelinating form, has been found to result from mutations in the myelin protein zero (MPZ) gene (Hayasaka *et al.*, 1993). Disease in another group of patients results from mutations of the connexin 32 (Cx32) gene (Bergoffen *et al.*, 1993; Ionasescu *et al.*, 1994, 1996). These three genes encoding myelin-related proteins are the major causes of CMT with demyelination. Recently, rare gene mutations in the early growth response protein (EGR2), myotubularin-related protein 2 (MTMR2), N-myc downstream-regulated gene 1 (NDRG-1), periaxin (PRX) and ganglioside-induced differentiation-associated protein 1 (GDAP1) genes have been found in patients with the demyelinating form (Warner *et al.*, 1998; Bolino *et al.*, 2000; Kalaydjieva *et al.*, 2000; Guilbot *et al.*, 2001; Nagarajan *et al.*, 2001; Yoshihara *et al.*, 2001; Baxter *et al.*, 2002). Several genes causing CMT type 2 have also been identified, including neurofilament L (NF-L) the kinesin motor superfamily (KIF1Bb) and lamin A/C nuclear envelope proteins, as well as GDAP1 (Mersiyanova *et al.*, 2000; Zhao *et al.*, 2001; De Sandre-Giovannoli *et al.*, 2002; Cuesta *et al.*, 2002).

CMT phenotypes caused by different gene abnormalities have been widely analysed, but no firm consensus has been established (Boerkoel *et al.*, 2002). In patients with Cx32 mutations, some authors considered the demyelinating process to predominate (Scherer, 1999; Scherer and Fischbeck, 1999; Tabaraud *et al.*, 1999; Gutierrez *et al.*, 2000), while others favoured a primarily axonal neuropathy (Hahn *et al.*, 1990, 2001; Birouk *et al.*, 1998; Senderek *et al.*, 1999). As for MPZ mutations, several families with an axonal phenotype have been reported (Gabreels-Festen *et al.*, 1996; Marrosu *et al.*, 1998; Chapon *et al.*, 1999; De Jonghe *et al.*, 1999; Misu *et al.*, 2000; Boerkoel *et al.*, 2002), suggesting a subgroup of patients with MPZ mutations causing a primarily axonal neuropathy. Wide variation has been shown in pathological findings, nerve conduction data, axonal and demyelinating severity, associated symptoms and prognosis in patients with MPZ, Cx32 and PMP22 gene abnormalities (Killian *et al.*, 1996; Birouk *et al.*, 1997, 1998; Thomas *et al.*, 1997; Senderek *et al.*, 1999; Dubourg *et al.*, 2001*a*; Boerkoel *et al.*, 2002). Phenotypic variation and the underlying gene abnormalities remain to be defined.

Axonal involvement has been reported in CMT1A, a demyelinating form (Dyck *et al.*, 1989; Garcia *et al.*, 1998; Krajewski *et al.*, 2000), as evidenced by decreased amplitude of muscle action potentials and by pathological abnormalities

(Dyck *et al.*, 1993; Garcia *et al.*, 1998; Krajewski *et al.*, 2000). In CMT1 patients, axonal involvement progressed in a time-dependent manner during a longitudinal study (Dyck *et al.*, 1989). Furthermore, conduction velocity and amplitude or neuropathic deficits at the first and last examinations in CMT1 were significantly correlated, suggesting an association between early slowing of conduction and subsequent neuropathic disability (Dyck *et al.*, 1989). These observations suggest that axonal involvement related to disease progression in demyelinating neuropathy is clinically important. However, demyelinating and axonal features that alter as disease progresses have not been assessed conclusively in CMT, particularly in forms other than CMT1A.

In addition, most studies of CMT phenotypic–genotypic variation have been performed in Caucasian populations; thus, features of CMT phenotypic–genotypic variation in Asian populations have not been elucidated. The frequency distribution of the breakpoint for PMP22 duplication at the CMT1A-REP (repeat) in 17p11.2 has been documented to be very similar among Caucasian and Asian populations (Yamamoto *et al.*, 1997), while the prevalence of CMT1A in the Japanese population has been considered to be extremely low compared with frequencies in Caucasians, although definitive comparative epidemiological studies have not been reported.

We therefore conducted a clinical, electrophysiological, histopathological and genetic study of 205 Japanese CMT patients with one of the three most common causative gene abnormalities, viz. abnormalities of PMP22, MPZ and Cx32, which involve major myelin-related proteins. We focused particularly on the demyelinating and axonal phenotypic features of these CMT patients.

## Patients and methods

### *Patients and DNA diagnosis*

Two hundred and five CMT patients from 124 families with a DNA diagnosis of PMP22 duplication (118 patients from 74 families), MPZ mutations (45 patients from 26 families) or Cx32 mutations (42 patients from 24 families; male only) were registered by the Study Group for Hereditary Neuropathy in Japan, working under the auspices of the Ministry of Health, Labour and Welfare of Japan. In the case of Cx32 mutations, gender effects on phenotypic expression are known to be profound (Nicholson and Nash, 1993; Birouk *et al.*, 1998; Dubourg *et al.*, 2001*b*), so only male patients were selected for our genotype–phenotype analysis. DNA analysis was performed in the Department of Neurology, Nagoya University Graduate School of Medicine, the Department of Pediatrics, Yamagata University School of Medicine, the Department of Neurology, Kagoshima University School of Medicine, or the Department of Neurology, Osaka University School of Medicine. In most cases, the PMP22 duplication was detected by Southern analysis, probing with PMP22 cDNA, the polymorphic markers VAW409R3 and EW401, and the CMT1A-REP fragments (Ikegami *et al.*, 1997; Yamamoto *et al.*, 1997, 1998). Hybridization with the probes pNEA102, pHK1.0P and pHK5.2P, mapping within the CMT1A-REP, was used to determine the location of crossover breakpoints, which were clustered in a 700-base pair (bp) region of the CMT1A-REP. Quantitation of hybridized signals for each band was performed to evaluate duplicate gene dosage using a phosphor-image analyser (BAS-2000II; Fujix, Tokyo, Japan). In some cases, fluorescence *in situ* hybridization (FISH) was employed to detect PMP22 gene duplication.

A non-isotopic RNase cleavage assay (NIRCA) was employed as a screening test for MPZ and Cx32 mutations using a method described previously (Yoshihara *et al.*, 2000). The MPZ and Cx32 genes, separated into three and two fragments respectively, were amplified with the polymerase chain reaction (PCR). Sequences of the forward (F) and reverse (R) primers were as follows:

For the MPZ gene: F1, 5′-CTA GGG ATT TTA AGC AGG TTC C-3′ and R1, 5′-ATT GCT GAG AGA CAC CTG AGT CC-3′ for exon 1; F2, 5′-CCA TAG GTG CAT CTG ATT CC-3′ and R2, 5′-CCT CCT TAG CCC AAT TTA TC-3′ for exon 2; and F3, 5′-CAG CTG TGT TCT CAT TAG GGT CCT C-3′ and R3, 5′-GCT CAT CCT TTC GTA GCT CCA TCT C-3′ for exons 3–6. For the Cx32 gene: F4, 5′-AGT GAC AGG GAG GTG TGA ATG AG-3′ and R4, 5′-AGG GGT AGA CGT CGC ACT TGA C-3′ for part 1 of exon 2; and F5, 5′-TTT GAG GCC GTC TTC ATG TAT GTC-3′ and R5, 5′-AGT AGC CAG GGA AGG AAG GTT TTG-3′ for part 2 of exon 2.

The bacteriophage T7 promoter sequence 5′-TAA TAC GAC TCA CTA TAG GG-3′ was attached to each primer at the 5′ end. PCR amplification was performed using AmpliTaq Gold (Perkin Elmer, Wellesley, MA, USA). Initial amplification conditions were 95°C for 9 min for denaturation, followed by 35 cycles of denaturing at 95°C for 1 min, annealing at 60°C for 1 min and elongation at 72°C for 2 min. NIRCA was performed using a MutationScreener kit (Ambion, Austin, TX, USA) according to the manufacturer's protocol. This assay system is based on the properties of the RNase enzyme that cleaves single base-pair mismatches of hybridized RNA duplexes produced *in vitro* by generating sense and antisense transcripts of each PCR product using the specific primer pairs. The bacteriophage RNA T7 promoter sequence integrated into the forward and reverse primers allowed the PCR products to be converted to RNA. Sense and antisense RNA transcripts were hybridized, and RNA–RNA hybrids were then treated with an optimized RNase mixture (RNase I and RNase T1) to cleave the duplexes at the mismatch positions. RNase-digested products were electrophoresed through 2.5% agarose gels. PCR products were purified from the unreacted primers and nucleotides using a QIAquick PCR Purification kit (Qiagen, Valencia, CA, USA) according to the manufacturer's protocol. Duplicate amplifications analysed by NIRCA were performed to avoid false-positive results arising from PCR errors. Purified products

**Table 1** *Clinical features in 205 CMT patients with PMP22 duplication, MPZ mutations and Cx32 mutations*

| Clinical features | PMP22 duplication | MPZ mutations | | | Cx32 mutations |
|---|---|---|---|---|---|
| | | Total | MCV ≤38 m/s | MCV >38 m/s | |
| | ($n$ = 118) | ($n$ = 45) | ($n$ = 28) | ($n$ = 17) | ($n$ = 42) |
| Age (years) | 44.5 ± 19.2 | 36.9 ± 15.1 | 30.3 ± 15.1 | 48.8 ± 24.5 | 43.2 ± 21.4 |
| Age of onset (years) | 20.3 ± 16.3 | 20.9 ± 23.3 | 13.2 ± 15.3 | 34.0 ± 24.8 | 22.4 ± 19.0 |
| Disease duration (years) | 22.7 ± 17.3 | 15.2 ± 10.7 | 17.1 ± 13.5 | 14.8 ± 11.9 | 17.5 ± 19.8 |
| Sex, male/female ($n$) | 58/60 | 20/35 | 13/15 | 7/10 | 42/0 |
| Muscle weakness: $n$ (%) | 118 (100) | 45 (100) | 28 (100) | 17 (100) | 42 (100) |
| Muscular atrophy: $n$ (%) | 98 (83) | 39 (86) | 24 (86) | 15 (88) | 36 (86) |
| Muscular hypertrophy: $n$ (%) | 5 (4) | 3 (7) | 2 (7) | 1 (6) | 0 (0) |
| Sensory impairment: $n$ (%) | 105 (89) | 40 (89) | 25 (89) | 15 (88) | 36 (86) |
| Areflexia: $n$ (%) | 118 (100) | 32 (71) | 22 (78) | 10 (59) | 34 (81) |
| Associated symptoms: $n$ (%) | | | | | |
| Deafness | 2 (2) | 7 (16) | 2 (7) | 5 (29) | 4 (9) |
| Pupillary abnormality | 0 (0) | 8 (18) | 2 (7) | 6 (35) | 3 (7) |
| Scoliosis | 6 (5) | 6 (13) | 3 (11) | 3 (17) | 2 (5) |
| Dementia | 0 (0) | 0 (0) | 0 (0) | 0 (0) | 1 (2) |
| Serum CK elevation: $n$ (%) | 4 (3) | 14 (30) | 6 (21) | 8 (47) | 9 (21) |
| CSF protein elevation: $n$ (%) | 61 (52) | 34 (76) | 21 (75) | 13 (76) | 16 (38) |
| ADL score (modified Rankin score): $n$ (%) | | | | | |
| 0 | 74 (62) | 22 (50) | 15 (53) | 7 (41) | 4 (9) |
| 1 | 32 (26) | 11 (24) | 9 (32) | 2 (12) | 30 (72) |
| 2 | 5 (6) | 5 (11) | 3 (11) | 2 (12) | 2 (5) |
| 3 | 4 (5) | 6 (13) | 1 (4) | 5 (29) | 3 (7) |
| 4 | 1 (1) | 1 (2) | 0 (0) | 1 (6) | 3 (7) |
| 5 | 0 (0) | 0 (0) | 0 (0) | 0 (0) | 0 (0) |

For Cx32 mutations, male patients were selected. ADL = activities of daily living.

were sequenced directly using a Thermo Sequenase Cy5.5 terminator cycle sequencing kit (Amersham Biosciences, Piscataway, NJ, USA) and analysed with a GeneRapid sequencer system (Amersham, Pharmacia). In some cases, FISH was employed to detect PMP22 gene duplication. As the patients with point mutations of the PMP22 gene are not included in this paper, 'PMP22 mutation' means 'PMP22 duplication'.

Informed consent was granted by subjects beforehand according to the guidelines of the Ethics Committee of Nagoya University Graduate School of Medicine or those of the regional ethics committee for each institution.

## *Clinical assessment*

Clinical information was assessed in a standardized manner, including motor and sensory impairment, deep tendon reflexes, muscular atrophy or hypertrophy, foot deformity and autonomic impairment. Weakness was assessed in proximal muscles (deltoid, biceps, triceps muscles in the arm; iliopsoas, quadriceps muscles in the legs) as well as distal muscles (thenar, interosseous, finger flexion muscles in the arms; ankle dorsiflexion and toe dorsiflexion muscles in the legs) according to UK Medical Research Council (MRC) criteria (Hattori *et al.*, 1999). Impairment was assessed for various sensory modalities (vibration, joint position, pain and light touch) as mild, moderate or severe. Associated findings, including deafness, pupillary abnormalities, scoliosis and dementia, were also assessed. Routine blood chemistry results were reviewed, as were those of CSF analysis and cranial and limb MRI. Detailed family histories were obtained.

Ability to carry out activities of daily living was evaluated according to the modified Rankin scale as follows: 0, normal; 1, non-disabling symptoms not interfering with lifestyle; 2, minor disability from symptoms leading to some restrictions of lifestyle but not interfering with patients' capacity to look after themselves; 3, moderate disability from symptoms that significantly interfered with lifestyle or prevented fully independent existence; 4, moderately severe disability from symptoms that clearly precluded independent existence, although patients did not need constant attention day and night; 5, severe disability involving total dependence, including constant care day and night.

## *Electrophysiological analysis*

Nerve conduction was assessed for the median, ulnar, tibial and sural nerves. Recordings were performed by standard methods using surface stimulating and recording electrodes (Hattori *et al.*, 1999; Misu *et al.*, 1999, 2000; Koike *et al.*, 2001). Motor nerve conduction velocity (MCV), distal motor latency (DL) and compound muscle action potential (CMAP) were recorded for the median, ulnar and tibial nerves. Sensory nerve conduction velocity (SCV) and sensory nerve action potential (SNAP) were assessed for the median and sural nerves.

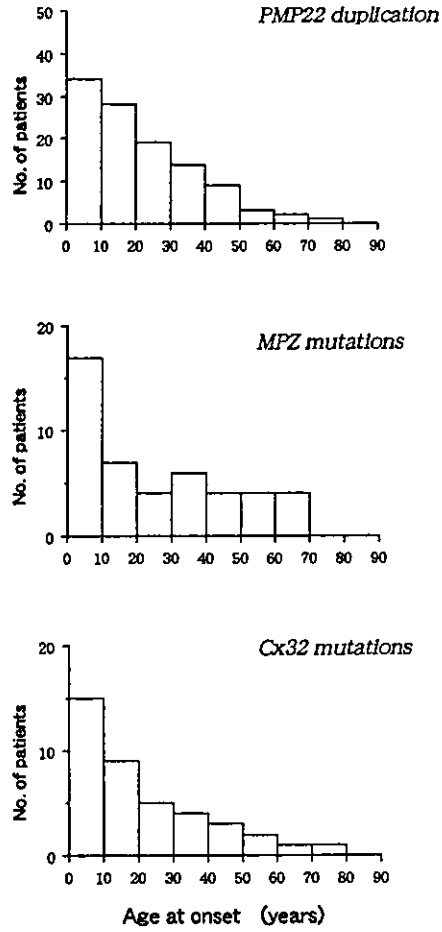


**Fig. 1** Frequency distribution of age at onset in CMT patients with PMP22 duplication, MPZ mutations and Cx32 mutations.

## *Pathological study*

Sural nerve biopsy was performed in 44 patients. Specimens were processed for glutaraldehyde-fixed, epoxy resin-embedded semithin sections and formalin-fixed, paraffin-embedded sections. Electron microscopic observations and teased-fibre studies were also performed in some cases. The morphometric pathological assessment of all nerve biopsy specimens was performed at the Department of Neurology, Nagoya University Graduate School of Medicine, according to the previously described methods (Sobue *et al.*, 1990; Misu *et al.*, 1999; Hattori *et al.*, 1999). Sural nerve biopsy was performed essentially as described previously (Sobue *et al.*, 1990; Hattori *et al.*, 1999; Misu *et al.*, 1999). Specimens were fixed in 2% glutaraldehyde in 0.025 M cacodylate buffer at pH 7.4, and processed for semithin, ultrathin or teased-fibre studies. Density of myelinated fibres was assessed directly from the toluidine blue-stained semithin transverse sections of sural nerves using a computer-assisted image analyser (Luzex FS; Nikon, Tokyo, Japan) as described previously (Sobue *et al.*, 1989, 1990, 1997). Unmyelinated fibre density was assessed using the same system, from electron microscopic photographs at ×10 000 magnification, taken to randomly cover uranyl acetate-stained ultrathin transverse sections (Sobue *et al.*, 1989; Hattori *et al.*, 1999). Isolated single nerves were prepared for teased-fibre analysis, in which the pathological condition of each fibre was evaluated according to criteria described previously (Sobue *et al.*, 1989; Dyck *et al.*, 1993). Part of the biopsy specimen was fixed in 10% buffered formalin solution, embedded in paraffin, and observed using haematoxylin and eosin staining as well as Klüver–Barrera staining.

Axonal and demyelinating features of sural nerve pathology were assessed as follows. We took axonal loss, axonal sprouts and axonal pathology in the teased-fibre preparations as axonal histopathological features. Clusters of two or more small myelinated fibres surrounded by basal lamina were designated as axonal sprouts, as described previously (Koike *et al.*, 2001; Vital *et al.*, 2001). Such sprouting is considered a marker of axonal neuropathy (Dyck *et al.*, 1993; De Jonghe *et al.*, 1999; Misu *et al.*, 2000; Vital *et al.*, 2001). Hypertrophic changes of nerve fascicles, onion bulbs, tomacula or globule formation and demyelinating pathology in teased nerve fibre preparations were taken as demyelinating features (Sobue *et al.*, 1990, 1997; Dyck *et al.*, 1993; Sander *et al.*, 1998, 2000).

## *Statistical analysis*

Clinical, electrophysiological and pathological data were compared using the $\chi^2$ test and the Mann–Whitney $U$ test. ANOVA (analysis of variance) with a two-way Student $t$-test was used for continuous variables with a normal distribution. Correlation studies were performed using Spearman's regression analysis. Statistical significance was considered to exist when the $P$ value $< 0.05$.

# Results

## *Patients with PMP22 duplication, MPZ mutations and Cx32 mutations*

Clinical features of 205 CMT patients are summarized in Table 1. The mean age at examination, age at onset and duration of illness were essentially similar in the three groups with PMP22 duplication, MPZ mutations and Cx32 mutations. An age of onset <10 years was most frequent for all mutations, but the distribution pattern of age at onset was different among the three gene abnormalities. A gradual unimodal decrease with advancing age was seen for PMP22 duplication and Cx32 mutations, and a rather diffuse distribution among all ages was seen for MPZ mutations (Fig. 1). The male-to-female ratio was nearly equal for PMP22 duplication and MPZ mutations; for Cx32 mutations, only male patients were selected. Muscle weakness and atrophy, predominantly in the lower legs in a distally accentuated pattern, was common to PMP22 duplication, MPZ mutations and Cx32 mutations. Muscle hypertrophy,

**Table 2** *Nerve conduction study in 205 CMT patients with PMP22 duplication, MPZ mutations and Cx32 mutations*

| Mutations | | MCV | | | | SCV | | |
|---|---|---|---|---|---|---|---|---|
| | | MCV m/s | DL ms | CMAP mV | Range | SCV (m/s) | SNAP (μV) | Range |
| PMP22 duplication | ($n$ = 118) | | | | | | | |
| Median | ($n$ = 117) | 21.1 ± 5.7 | 10.3 ± 2.6 | 3.3 ± 2.8 | (0–12.3) | 21.0 ± 7.3 | 0.9 ± 4.2 | (0–17.0) |
| Tibial | ($n$ = 54) | 20.2 ± 6.2 | 11.2 ± 6.2 | 1.2 ± 2.0 | (0–9.3) | | | |
| Sural | ($n$ = 83) | | | | | 20.4 ± 11.4 | 0.7 ± 0.2 | (0–14.5) |
| MPZ mutations | ($n$ = 45) | | | | | | | |
| ≤38m/s | | | | | | | | |
| Median | ($n$ = 28) | 16.5 ± 7.0 | 8.7 ± 3.5 | 8.1 ± 5.4 | (0.8–18.1) | 21.8 ± 5.4 | 2.7 ± 3.7 | (0–10.5) |
| Tibial | ($n$ = 19) | 21.7 ± 11.1 | 15.3 ± 7.4 | 0.9 ± 1.2 | (0–4.0) | | | |
| Sural | ($n$ = 16) | | | | | 26.3 ± 6.1 | 2.0 ± 2.0 | (0–4.2) |
| >38m/s | | | | | | | | |
| Median | ($n$ = 17) | 44.3 ± 4.7 | 3.9 ± 1.6 | 3.3 ± 3.7 | (0–11.0) | 51.0 ± 5.7 | 0.8 ± 0.9 | (0–2.8) |
| Tibial | ($n$ = 11) | 34.8 ± 3.2 | 7.7 ± 2.5 | 0.6 ± 0.8 | (0–2.3) | | | |
| Sural | ($n$ = 10) | | | | | 51.5 ± 2.1 | 0.3 ± 0.6 | (0–2.2) |
| Cx32 mutations | ($n$ = 42) | | | | | | | |
| Median | ($n$ = 42) | 33.2 ± 5.7 | 5.3 ± 1.7 | 2.0 ± 1.8 | (0–8.1) | 38.6 ± 6.4 | 4.4 ± 3.8 | (0–14.2) |
| Tibial | ($n$ = 17) | 22.3 ± 5.7 | 6.1 ± 2.5 | 1.1 ± 1.7 | (0–6.0) | | | |
| Sural | ($n$ = 16) | | | | | 36.5 ± 8.6 | 1.8 ± 3.3 | (0–12.0) |
| Controls | ($n$ = 121–191) | | | | | | | |
| Median | ($n$ = 191) | 57.8 ± 3.7 | 3.3 ± 0.4 | 16.4 ± 5.3 | (9.5–23.5) | 57.8 ± 4.7 | 35.2 ± 12.6 | (18.3–39.5) |
| Tibial | ($n$ = 121) | 46.9 ± 3.5 | 4.6 ± 0.8 | 16.3 ± 5.8 | (9.2–24.4) | | | |
| Sural | ($n$ = 133) | | | | | 51.0 ± 5.1 | 17.3 ± 7.1 | (8.9–25.7) |

Data are mean ± standard deviation. Ranges of CMAP and SNAP values are shown in parentheses. Control values are those described previously (Koike *et al.*, 2001; Misu *et al.*, 1999, 2000).

particularly in the calf muscle, was seen in five patients with PMP22 duplication and three patients with MPZ mutations. Sensory impairment for all modalities was pronounced in the distal legs, and areflexia mainly in the lower legs was common in all three gene abnormalities. Associated symptoms of deafness, pupillary abnormality and scoliosis, which were present for all three gene abnormalities, were more frequent for MPZ and Cx32 mutations. Serum creatine kinase (CK) elevation was also more frequently observed for MPZ and Cx32 mutations than for PMP22 duplication. CSF protein elevations were present in 38–76% of patients, particularly in those with MPZ mutations. The modified Rankin score showed that 88, 74 and 81% of patients with PMP22 duplication, MPZ mutations and Cx32 mutations, respectively, were normal or non-disabled with respect to daily life (score 0 or 1), while 6, 15 and 14% of patients, respectively, were moderately or moderately severely disabled (score 3 or 4).

## *Electrophysiological findings*

Mean MCVs in the median and tibial nerves and mean SCVs in the median and sural nerves were uniformly reduced in all three mutations, except for a subgroup of patients with MPZ mutations (Table 2). Distal latency was markedly prolonged for PMP22 duplication and the subgroup with MPZ mutations, but less markedly prolonged for Cx32 mutations and other subgroups with MPZ mutations (Table 2). Mean CMAPs and SNAPs were markedly reduced in all nerves, particularly in the lower legs, for all three gene abnormalities (Table 2). The shape and duration of proximal and distal CMAPs were similar, demonstrating absence of conduction block or temporal dispersion in all three gene abnormalities.

In PMP22 duplication, the median nerve MCVs were markedly reduced below 38 m/s, and the distribution of MCVs was unimodal, peaking at 21.1 m/s (Fig. 2). In Cx32 mutations, the distribution of median MCVs was also unimodal, peaking at 33.2 m/s with a range of 22.8–46.6 m/s (Fig. 2). In MPZ mutations, the median nerve MCVs were distributed in a bimodal pattern, representing two subgroups with MCV either >38 m/s or ≤38 m/s (Fig. 2). Distal latencies were significantly less prolonged, and CMAPs and SNAPs were significantly more decreased in the subgroup with median nerve MCV >38 m/s (Table 2). These findings suggested two distinctive subgroups of MPZ mutations with either demyelinating or axonal phenotypes: MCV >38 m/s, showing an axonal phenotype, and MCV ≤38 m/s, showing a demyelinating phenotype. Several clinical features differed between the above-mentioned MPZ mutation subgroups (Table 1). Patients with MCV >38 m/s were older at onset than those with MCV ≤38 m/s, and in the former group family neuropathic sign was often not apparent. Associated symptoms of sensorineural deafness and pupillary abnormality (Adie's pupil) were more frequent in patients in the former, axonal subgroup than in the latter, demyelinating subgroup. Considerable serum CK elevation

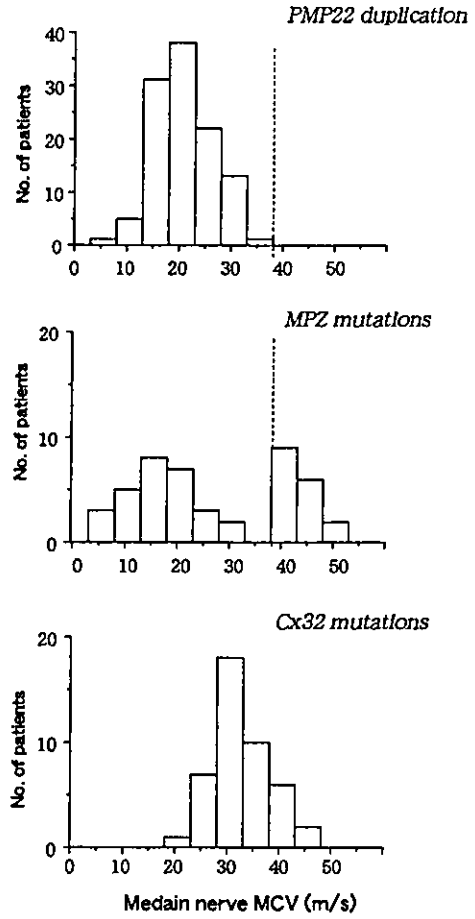


**Fig. 2** Frequency distribution of median nerve MCVs in CMT patients with PMP22 duplication, MPZ mutations and Cx32 mutations.

was also more frequent in the axonal subgroup. Other motor and sensory symptoms did not differ significantly between the two subgroups (Table 1). These associated symptoms were seen in association with several types of MPZ mutations.

## *Pathology of the sural nerve*

In PMP22 duplication, myelinated fibre density was variably reduced, ranging from 183 to 6854/mm$^2$ (Table 3, Fig. 3). Unmyelinated fibre density was also variably reduced but relatively preserved, ranging from 16 157 to 28 160/mm$^2$. Fibres showing demyelinating pathology in teased-fibre preparations represented 80.1 ± 17.7% of the total, while axonal pathology was seen in 0.7 ± 2.8%. Tomacula and globule formation in teased fibres was variable among patients, with a mean frequency of 7.3 ± 6.5% of fibres (Fig. 4). Onion bulbs were present to varying degrees, ranging from 10 to 83% of myelinated fibres, appearing in half of the myelinated fibres and showing a mean of 3.94 lamellae (Table 3, Fig. 3). Axonal sprouts were generally rare, but in some patients axonal sprouts were abundant (Table 3, Fig. 3). These findings indicate that in PMP22 duplication demyelinating pathology was predominant, while axonal loss and axonal sprouts were variably present.

In MPZ mutations, myelinated and unmyelinated fibre densities were also variable, ranging from 510 to 8279/mm$^2$ and 10 387 to 36 874/mm$^2$, respectively (Table 3). The frequency of demyelinating and axonal pathology was significantly variable among individual patients. When patients were subdivided into those with median nerve MCV ≤38 m/s (demyelinating) and those with higher MCV (axonal), myelinated fibre densities were significantly lower in the demyelinating subgroup than in the axonal subgroup ($P < 0.05$; Table 3), while unmyelinated fibre density did not differ significantly between subgroups (Table 3, Fig. 3). The frequencies of fibres with demyelinating pathology, tomacula and globule formation, and onion bulbs were significantly greater in the demyelinating subgroup ($P < 0.0001$, $P < 0.001$ and $P < 0.05$, respectively). An uncompacted myelin sheath was occasionally observed. In contrast, the frequency of fibres with axonal pathology and the density of axonal sprouts were significantly greater in the axonal subgroup ($P < 0.01$ and $P < 0.05$, respectively; Table 3, Fig. 4). In individual patients with MPZ mutations, pathological features in which either demyelinating or axonal involvement was predominant, combined or concomitant demyelinating and axonal pathological findings were rare. Thus, pathological features were distinctive between the demyelinating and axonal subgroups defined by median nerve MCV.

In Cx32 mutations, myelinated fibre density was diminished, but less markedly than in PMP22 duplications and MPZ mutations (Table 3). Unmyelinated fibres were also relatively well preserved (Table 3). Less marked reduction in the myelinated and unmyelinated fibre density reflected the frequent presence of axonal sprouts (Table 3, Fig. 3). Teased-fibre preparations showed fibres with demyelinating and axonal pathologies, but both were mild. Globule and tomacula formation and onion bulb formation were also mild (Table 3, Fig. 4). However, axonal sprouts were frequent, ranging from 340 to 2610/mm$^2$ (Table 3). Large myelinated axon loss and axonal sprouts were variable among the patients. Axonal and demyelinating pathologies were invariably present in combination in individual patients, although axonal features were predominant.

## *Median nerve MCVs, CMAPs and sural nerve pathology in relation to disease advancement*

In PMP22 duplication, slowed median MCV (≤38 m/s) was seen for all ages at examination (Fig. 5A) and durations of illness (data not shown). Median nerve CMAPs tended to decrease with advancing age ($r = 0.28$, $P < 0.013$; Fig. 5A) and with disease duration (not significant; data not shown). In Cx32 mutations, moderately slowed MCV (22.8–46.6 m/s)

**Table 3** *Pathological features of sural nerves in 44 CMT patients*

| Mutations | Myelinated fibre density (no./mm²) | Unmyelinated fibre density (no./mm²) | Teased-fibre study | | |
|---|---|---|---|---|---|
| | | | De-/remyelination (%) | Axonal (%) | Globule/tomacula (%) |
| PMP22 duplication ($n$ = 23) | 2612 ± 2348 (183–6854) | 20 196 ± 5658 (16 157–28 160) | 80.1 ± 17.7 (39–100) | 0.7 ± 2.8 (0–3.5) | 7.3 ± 6.5 (0–18) |
| MPZ mutations ($n$ = 11) | 2208 ± 1864 (501–8279) | 22 197 ± 8452 (10 387–36 874) | 65.6 ± 39.2 (5–94) | 1.9 ± 2.1 (0–5) | 3.9 ± 2.6 (0–7) |
| MCV ≤38 m/s ($n$ = 6) | 1146 ± 646 * | 18 742 ± 7487 NS | 85.0 ± 18.7 *** | 1.2 ± 1.8 ** | 5.4 ± 4.0 ** |
| MCV >38 m/s ($n$ = 5) | 4631 ± 844 * | 26 515 ± 8426 NS | 7.5 ± 3.5 *** | 4.0 ± 1.4 ** | 0.3 ± 0.9 ** |
| Cx32 mutations ($n$ = 10) | 6090 ± 1158 (4176–12 711) | 34 705 ± 9053 (25 165–43 175) | 9.2 ± 6.4 (1–18) | 4.2 ± 2.4 (1–7) | 3.0 ± 2.3 (0–4) |
| Controls ($n$ = 9) | 8190 ± 511 | 29 913 ± 3457 | 3.8 ± 2.2 | 0.5 ± 0.8 | 0 |

| Mutations | Onion bulbs | | Axonal sprouts (no./mm²) | G ratio |
|---|---|---|---|---|
| | Rate (no./MFD) | Lamellae (no./mm²) | | |
| PMP22 duplication ($n$ = 23) | 0.47 ± 0.29 (0.10–0.83) | 3.94 ± 1.46 (1–6) | 160 ± 210 (10–1085) | 0.68 ± 0.05 (0.59–0.79) |
| MPZ mutations ($n$ = 11) | 0.22 ± 0.23 (0.03–0.80) | 2.31 ± 1.20 (1–4) | 350 ± 410 (0–1190) | 0.71 ± 0.04 (0.64–0.76) |
| MCV ≤38 m/s ($n$ = 6) | 0.36 ± 0.22 * | 2.97 ± 0.35 * | 30 ± 20 * | 0.70 ± 0.04 NS |
| MCV >38 m/s ($n$ = 5) | 0.05 ± 0.07 * | 1.00 ± 0.00 * | 730 ± 290 * | 0.74 ± 0.02 NS |
| Cx32 mutations ($n$ = 10) | 0.06 ± 0.04 (0.04–0.14) | 2.39 ± 0.26 (2–3) | 1090 ± 830 (340–2610) | 0.70 ± 0.05 (0.63–0.75) |
| Controls ($n$ = 9) | 0 | – | <20 | 0.6–0.7 |

Data are mean ± standard deviation. Ranges are shown in parentheses. Control values are those described previously (Sobue, *et al.* 1989). *$P$ < 0.01; **$P$ < 0.001; ***$P$ < 0.0001; NS = not significant.

was noted consistently for all ages at examination (Fig. 5A) as well as disease durations (data not shown). Median nerve CMAPs decreased with age ($r$ = 0.45, $P$ < 0.0013; Fig. 5A), and tended to decrease with duration of illness (not significant; data not shown). In MPZ mutations, however, two subgroups of MCVs were consistently present through all ages at examination (Fig. 5A) and durations of illness (data not shown). No tendency for CMAPs to decrease with advancing age or disease duration was observed (Fig. 5A).

Sural nerve pathology also changed markedly with disease advancement (Fig. 5B). In the PMP22 duplication, myelinated fibre density, in particular that of large myelinated fibres, decreased significantly with increasing age at examination ($r$ = 0.71, $P$ < 0.0001; Fig. 5B) and duration of illness ($r$ = 0.40, $P$ < 0.001; data not shown). Onion bulbs were rare in young patients, but their frequency increased with advancing age ($r$ = 0.42, $P$ < 0.01; Fig. 5B). In Cx32 mutations, large myelinated fibre density was relatively preserved in the younger patients, but decreased markedly with advancing age ($r$ = 0.81, $P$ < 0.001; Fig. 5B) and duration of illness ($r$ = 0.37, $P$ < 0.05; data not shown). Axonal sprouts were more frequent in older patients, and the density of axonal sprouts correlated well with age at examination ($r$ = 0.68, $P$ < 0.01; Fig. 5B) and duration of illness ($r$ = 0.43, $P$ < 0.01; data not shown). In cases with MPZ mutations, two small but distinctive subgroups were present, and were difficult to assess.

The MCV slowing was consistently preserved in spite of pathological changes in sural nerves in patients with PMP22 duplication and Cx32 mutations (Fig. 6). Median nerve MCVs were consistently slowed independently of large myelinated fibre loss, degree of onion bulb formation and axonal sprouts in the sural nerves (Fig. 6).

The findings indicate that MCVs in these three main genetic groups are consistently preserved independently of age at examination and disease duration; in patients with PMP22 duplication and Cx32 mutations, slowed MCVs are consistently preserved independently of the development of pathological changes. In contrast, CMAPs and large myelinated fibre populations tended to decrease with advancing age and disease duration. In cases with MPZ mutations, two relatively small but distinct subgroups with different MCVs were present, and tendencies related to age, disease duration and pathology were difficult to assess.

## *Concordance and discordance in MCVs among siblings, and gene mutations*

In PMP22 duplication, all patients showed MCVs ≤38 m/s, though the extent of MCV reduction was variable. MCVs of